Neuropharmacology 252 (2024) 109940

Contents lists available at ScienceDirect

Neuropharmacology

journal homepage: www.elsevier.com/locate/neuropharm

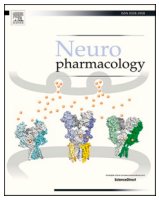

# Pharmacological blockade of 2-AG degradation ameliorates clinical, neuroinflammatory and synaptic alterations in experimental autoimmune encephalomyelitis

Livia Guadalupi [a,b,1], Georgia Mandolesi [b,c,1], Valentina Vanni [b], Sara Balletta [d], Silvia Caioli [d], Anto Pavlovic [f], Francesca De Vito [d], Diego Fresegna [a,b], Krizia Sanna [a], Laura Vitiello [c,f], Monica Nencini [b], Alice Tartacca [a], Fabrizio Mariani [a], Valentina Rovella [a], Sven Schippling [e], Iris Ruf [e], Ludovic Collin [e], Diego Centonze [a,d,*], Alessandra Musella [b,c]

[a] Department of Systems Medicine, University of Rome Tor Vergata, Rome, Italy
[b] Synaptic Immunopathology Lab, IRCCS San Raffaele Roma, Rome, Italy
[c] Department of Human Sciences and Quality of Life Promotion University of Rome San Raffaele, Italy
[d] IRCCS Istituto Neurologico Mediterraneo (INM) Neuromed, Pozzilli (IS), Italy
[e] F. Hoffmann -La Roche Ltd. Roche. Innovation Center Basel, Switzerland by Roche Pharma Research and Early Development (pRED), Roche Innovation Center Basel, 4070 Basel, Switzerland
[f] Laboratory of Flow Cytometry, IRCCS San Raffaele Roma, Rome, Italy

ARTICLE INFO

Handling Editor: Dr M. Roberto

*Keywords:*
Multiple sclerosis (MS)
Microglia
Neuroinflammation
Synaptic transmission
Excitotoxicity
Endocannabinoid
Monoacylglycerol lipase (MAGL)

ABSTRACT

The endocannabinoid system (ECS) is critically involved in the pathophysiology of Multiple Sclerosis (MS), a neuroinflammatory and neurodegenerative disease of the central nervous system (CNS). Over the past decade, researchers have extensively studied the neuroprotective and anti-inflammatory effects of the ECS. Inhibiting the degradation of the endocannabinoid 2-arachidonoylglycerol (2-AG) has emerged as a promising strategy to mitigate brain damage in MS.

In this study, we investigated the effects of a novel reversible MAGL inhibitor (MAGLi 432) on C57/BL6 female mice with experimental autoimmune encephalomyelitis (EAE), a model of MS. We assessed its implications on motor disability, neuroinflammation, and synaptic dysfunction. Systemic *in vivo* treatment with MAGLi 432 resulted in a less severe EAE disease, accompanied by increased 2-AG levels and decreased levels of arachidonic acid (AA) and prostaglandins (PGs) in the brain. Additionally, MAGLi 432 reduced both astrogliosis and microgliosis, as evidenced by decreased microglia/macrophage density and a less reactive morphology. Flow cytometry analysis further revealed fewer infiltrating $CD45^+$ and $CD3^+$ cells in the brains of MAGLi 432-treated EAE mice. Finally, MAGLi treatment counteracted the striatal synaptic hyperexcitability promoted by EAE neuroinflammation.

In conclusion, MAGL inhibition significantly ameliorated EAE clinical disability and striatal inflammatory synaptopathy through potent anti-inflammatory effects. These findings provide new mechanistic insights into the neuroprotective role of the ECS during neuroinflammation and highlight the therapeutic potential of MAGLi-based drugs in mitigating MS-related inflammatory and neurodegenerative brain damage.

## 1. Introduction

Multiple sclerosis (MS) is a chronic inflammatory disease affecting the central nervous system (CNS) and presenting both demyelinating and neurodegenerative features (Compston and Coles, 2008). Clinical and preclinical data revealed that lymphocyte infiltration, together with microglial and astroglial activation are key events in the onset and progression of the disease. The early stages of the disease are characterized by brain and spinal cord invasion by peripheral immune cells, including macrophages, $CD8^+$ T cells, $CD4^+$ T cells and B cells, while

* Corresponding author. Department of Systems Medicine, Tor Vergata University, Rome, Italy.
*E-mail address:* centonze@uniroma2.it (D. Centonze).
[1] Equal contribution.

https://doi.org/10.1016/j.neuropharm.2024.109940
Received 6 December 2023; Received in revised form 15 March 2024; Accepted 28 March 2024
Available online 2 April 2024

microglia and astrocyte activation are the main responsible of brain damage in the chronic phase (Dendrou et al., 2015; Baecher-Allan et al., 2018). Recent advances in MS and in its mouse model experimental autoimmune encephalomyelitis (EAE), clearly showed that neuroinflammation unbalances synaptic transmission towards more pronounced hyperexcitability, ultimately resulting in excitotoxic neurodegeneration (Mandolesi et al., 2015). Remarkably, inflammatory synaptopathy is an attractive therapeutic target in MS, since early synaptic alterations are potentially reversible.

Soluble mediators of inflammation released by infiltrating lymphocytes and by microglia/macrophages are master players of inflammatory synaptopathy. Accordingly, in the EAE striatum we observed that the two major proinflammatory cytokines, IL-1β and TNF, acting at pre- or postsynaptic sites respectively, enhance glutamatergic transmission and induce dendritic pathology (Centonze et al., 2009; Musumeci et al., 2011; Haji et al., 2012; Rossi et al., 2012). Endocannabinoids (eCBs), including 2-arachidonoylglycerol (2-AG), are endogenous lipid-derived messengers able to bind to two G protein-coupled receptors cannabinoid receptor 1 (CB1) and 2 (CB2) and to non-CB1/non-CB2 receptors such as TRPV channels (Piomelli, 2003; De Petrocellis and Di Marzo, 2009). In MS, dysregulation of the endocannabinoid system (ECS) is involved in the progression of the disease, and animal research supports the utility of cannabinoid compounds for MS treatment (Centonze et al., 2007a; Chiurchiù et al., 2018). Different therapeutic strategies can increase the eCB tone. Targeting the eCBs metabolism to indirectly manipulate this pro-homeostatic system is emerging as an important pharmacological strategy, which avoids the unwanted side effects of direct CB receptor agonists (Ciaramellano et al., 2023). Enhancing anandamide (AEA) tone by inhibiting its degradation by fatty acid amide hydrolase (FAAH) provided significant clinical and synaptic protection in EAE (Rossi et al., 2011), while the effects of 2-AG in EAE pathophysiology is less explored.

Numerous findings support monoacylglycerol lipase (MAGL) as an interesting target for the treatment of many pathological conditions, including MS (Deng and Li, 2020). MAGL is the major enzyme that controls the levels of 2-AG, and is expressed in neurons, astrocytes, oligodendrocytes, microglia and pericytes (Deng and Li, 2020; Kemble et al., 2022). Several highly potent and selective MAGL inhibitors (e.g., JZL184, KLM29 and MJN110) are available and considered as useful tools to explore a wide range of positive effects induced by 2-AG in animal models. JZL184, which acts as an irreversible inhibitor, was found to reduce demyelination in association with less microglia/macrophage activation in the spinal cord of EAE mice (Bernal-Chico et al., 2015), to control spasticity (Pryce et al., 2013), and to decrease neurological deficits (Kinsey et al., 2009; Long et al., 2009; Schlosburg et al., 2010; Bernal-Chico et al., 2015; Brindisi et al., 2016). Unfortunately, chronic administration of JZL184 led to a generalized desensitization of its central action, recapitulating the effects observed in mice lacking the MAGL gene (Schlosburg et al., 2010). For this reason, reversible MAGL inhibitors have been recently developed (Hernández-Torres et al., 2014; Tuccinardi et al., 2014; Deng and Li, 2020; Ren et al., 2020), in an attempt to take more advantage of 2-AG neuroprotective and anti-inflammatory effects. Since the molecular and cellular mechanisms underlying the potential beneficial effects of MAGL inhibition in EAE are still unclear, here we investigated the effect of a novel reversible MAGL inhibitor (MAGLi 432) (Kemble et al., 2022) in the context of EAE.

## 2. Materials and methods

### 2.1. Animals

Female C57BL/6 mice (6–8 weeks of age) were purchased from Charles-River (Italy) and stabilized, four-caged, in Type 3H cages for at least seven days after delivery. Mice were housed under constant conditions with a light/dark cycle of 12 h, in a temperature-controlled environment and free access to food and water. Animal experiments were carried out according to the Internal Institutional Review Committee, the European Directive 2010/63/EU and the European Recommendations 526/2007 and the Italian D. Lgs 26/2014. The experimental protocol was approved by the Italian Ministry of Health (Aut.n. 337/2021-PR). All efforts were made to minimize the number of animals used and their suffering. The choice of female sex is of relevance for MS, due to the high prevalence of the disease in female versus male subjects. All experiments were performed blind. A total of two independent immunizations of a minimum size of 9 animals per group were performed.

### 2.2. EAE induction and in vivo treatment

Chronic-progressive EAE was induced in eight-to ten-week-old mice by active immunization with an emulsion of myelin oligodendrocyte glycoprotein peptide 35–55 (MOG35-55) in Complete Freund's Adjuvant (CFA), followed by intravenous administration of pertussis toxin (400 ng) twice (at days 0 and 2) as previously described (Centonze et al., 2009). Control mice, hereafter referred to as CFA, received the same treatment as EAE mice without the MOG peptide, including complete CFA and Pertussis toxin. EAE clinical score was recorded daily according to a 0–5 scale. For each animal, the onset day was recorded as the day post-immunization (dpi) when it showed the first clinical manifestations (score >0). EAE mice were further randomly divided in two groups and were daily treated with the drug (MAGLi 432; i. p., 2 mg/kg/day) (Kemble et al., 2022) or vehicle (VHL, 80% NaCl 0.9% + 10% DMSO+10% Tween 80) via intraperitoneal injection at a volume of 200 μL/mouse, starting from 0-day post immunization (0 dpi). The clinical course of the disease was followed until the acute phase around 20–24 dpi (acute phase refers to the post peak symptomatic phase). Mice were killed after 1 h from MAGLi 432/VHL administration.

Healthy mice were treated with MAGLi 432 (2 mg/kg/day) or vehicle (VHL, 80% NaCl 0.9% + 10% DMSO+10% Tween 80) via intraperitoneal injection at a volume of 200 μL/mouse, 24 h and 2 h before the sacrifice.

### 2.3. Behavioral assessment

Animals were tested during the light period (9:00–12:00 a.m.) in a dedicated room with a constant temperature (26 ± 1 °C). Each session was preceded by at least 1 h habituation in the behavioral room.

#### 2.3.1. Grip strength test

Immunized mice were tested for grip strength performance using the Grip Strength Meter (Ugo Basile, Italy) at the onset of disease (8 and 14 dpi) and at the acute phase (21 dpi) (Mandolesi et al., 2019). The apparatus for this test consisted of a steel wire grid (8 × 8 cm) connected to an isometric force transducer Mice were lifted by their tail so that they grasped the grid with their paws. Then gently pulled backward until they released the grid and the maximal force in newtons (N) exerted by the mouse before losing the grip was measured. The mean of three consecutive measurements for each animal was calculated.

### 2.4. Immunofluorescence and confocal microscopy

Mice were deeply anesthetized and intracardially perfused with ice-cold 4% paraformaldehyde (PFA) at 24 dpi and at 35 dpi (N = 3–4 per group). Collected brains were post-fixed in 4% PFA for 2 h and equilibrated with 30% sucrose for at least one night. Thirty-micrometer-thick coronal sections were serially cut on a frozen microtome to include the whole striatum to perform immunofluorescence experiments as previously described (Mandolesi et al., 2019). Brain regions were identified using a mouse brain atlas, and for each animal, at least 6 serial sections (one section every six in the bregma interval from 1.34 to − 0,10) containing the striatum, were processed for immunofluorescence. Slices were permeabilized in PBS with Triton X-100 0.25% (Tx-PBS). All

following incubations were performed in Tx-PBS. To block non-specific sites, sections were pre-incubated with 10% normal donkey serum solution for 1 h RT and then incubated with the primary antibody overnight at + 4 °C. Then, after washing, they were incubated with secondary antibodies for 2 h RT and rinsed. Primary antibodies were used as follows: rabbit or Goat anti-IBA1 (1:750, Wako); Rabbit anti-TMEM119 (0.25 μg/mL, Abcam); Rabbit anti-GFAP (1:500, Dako); Rat anti-CD3 (1:300, R&D systems); Rabbit anti-Collagen IV (1:1000, Biorad). These were used in combination with the following secondary antibodies: Cy3-conjugated donkey anti-rabbit or anti-Goat (1:200; Jackson); Alexa-488-conjugated donkey anti-rabbit or anti-rat (1:200; Invitrogen), Alexa-647-conjugated donkey anti-rabbit (1:200; Invitrogen). Nuclei were stained with [4′, 6-diamidino-2-phenylindole (DAPI)] (1 μL/ml; Sigma Aldrich).

Images were acquired using a Nikon Eclipse TI2 confocal laser-scanner microscope with 20× and 40×, 60× objectives and were processed using ImageJ software. All images had a pixel resolution of 1024 × 1024. The confocal pinhole was kept at 1.0, the gain and the offset were lowered to prevent saturation in the brightest signals, and sequential scanning for each channel was performed. Z-stack acquisitions (20× and 40× objective, zoom 1× with 2 μm intervals for a total of 17 steps; 60×, zoom 2 with 1 μm intervals for a total of 34 steps) were made applying the same intensity and exposure time. A large image function generates a single high-magnification image (capturing 2 images, according to Bregma level). A z-projection image derived from all captured images was produced. All images were adjusted for reducing noise by applying smooth and background subtraction as required by the NIH ImageJ. In the z-projections, the IBA + density analysis to evaluate microglia density was performed and a bilateral Roi (region of interest) including dorsal striatum was drawn. To obtain cellular density, the number of IBA1+ cells was automatically determined, and divided by the area covered by the Roi. Data were expressed as the number of cells per $mm^2$. ImageJ software was used to define microglia morphology as in (Pinto et al., 2020). A gray scale image of IBA-1 was generated and then cells were cropped and thresholded to generate a binary (black and white) image (See) Supplementary Fig. 1. For the Sholl analysis the ImageJ plugin Sholl Analysis was used (starting radius: 2 μm, ending radius: 60 μm, radius step size: 2 μm). For skeleton analysis, the same binary image created for Sholl Analysis was used. The image was skeletonized using the ImageJ Plugin Skeletonize and was subsequently analysed using the plugin Analyze Skeleton 2D (Young and Morrison, 2018). ImageJ software was used to quantify the astroglia total area (GFAP + surface %) in the Roi, generating intensity threshold images (binary images), and the measure of astroglial surface was calculated by the software.

### 2.5. Electrophysiology

Mice (11–13 wks) were euthanized by cervical dislocation and the brains were removed. Then, corticostriatal coronal slices (200 μm) were cut by means of a vibratome (Leica VT1200 - Leica biosystems, Wetzlar, Germany) and transferred to a recording chamber with continuously flowing artificial CSF (ACSF) (34 °C, 2–3 mL/min) gassed with 95% $O_2$–5% $CO_2$. The composition of ACSF was (in mM): 126 NaCl, 2.5 kC l, 1.2 MgCl2, 1.2 NaH2PO4, 2.4 CaCl2, 11 Glucose, 25 NaHCO3. Whole-cell patch-clamp recordings were made with borosilicate glass pipettes (1.8 mm outer diameter; 2–4 MΩ), in voltage-clamp mode, at the holding potential of −80 mV. Only data from putative medium spiny projection neurons (MSNs). Spontaneous excitatory and inhibitory post-synaptic currents (EPSCs, IPSCs) recording, data storing, and analysis were performed as previously described (Gentile et al., 2016). Corticostriatal slices derived from EAE mice *in vivo* treated with MAGLi 432 or VHL (sEPSC, 20–24 dpi; sIPSC: 30–34 dpi) were used to record sEPSCs and sIPSCs. In some experiments, AM281 (2 μM; Sigma), a potent and selective CB1 antagonist, was acutely applied during the electrophysiological recordings.

For *ex vivo* experiments, sEPSCs were recorded from EAE corticostriatal slices (20–24 dpi) incubated with MAGLi 432 (1 μM, 1 h), or pre-incubated with AM281 and subsequently with AM281 plus MAGLi 432 (1 h). Synaptic events were stored using PCLAMP (Axon Instruments - Molecular Devices, San Jose, CA, USA) and analysed offline on a personal computer with Mini Analysis 6.0.7 (Synaptosoft, Leonia, NJ, USA) software.

### 2.6. Infiltrating mononuclear cell isolation

Mice were deeply anesthetized and intracardially perfused with ice-cold 1*X* PBS at 21–23 dpi (EAE VHL N = 12; EAE MAGLi N = 8). Collected brains and spinal cords of 2 mice for each experimental group were pooled and mechanically disaggregated. Cell suspension was passed through a 70-μm cell strainer to remove cell debris, centrifuged and subjected to a gradient separation. Cells were resuspended in 4 mL of 37% Percoll in room-temperature PBS and overlay onto 3 mL of 70% Percoll in room-temperature PBS in a 15 mL tube. Cells were centrifuged at 500 g for 30 min at room temperature without brake. The fat on top of the tube was removed and the cells from the interface were collected and the sample washed twice in PBS. Two pairs of samples were finally combined to obtain a single pool derived from 4 mice for each experimental group.

### 2.7. Flow cytometry

Immediately after isolation, CNS infiltrating immune cells were prepared for flow cytometric analysis. Cells were incubated with Zombie UV™ Fixable Viability kit (BioLegend, San Diego CA) according to manufacturer's instructions. Briefly, cells were washed in PBS and then resuspended in 100 μl of PBS diluted Zombie UV™ dye (diluted 1:100 from stock solution). Cells were incubated 15 min at room temperature in the dark, then washed with PBS 0.5% BSA. After staining with the vital dye, cells were labeled with fluorochrome-conjugated antibodies against membrane markers. The anti-mouse antibodies used were: anti-CD45 APC, anti-CD3 PE-Cy7, anti-CD4 APC-Cy7, anti-CD8a PE, anti-CD19 PE-Cy7, anti-F4/80 PE-CF594(all antibodies from BD Biosciences, Milan, Italy). Cells were incubated at 4 °C for 20 min in the dark with the appropriate mix of antibodies, then were washed and resuspended in PBS 0.5% BSA. Samples were acquired immediately on a BD LSR Fortessa X-20 and analysed using FACS Diva software (v8.0.2). At least 10000 events in the region of living (zombie uv negative) cells were acquired.

### 2.8. Liquid chromatography/mass spectrometry (LC/MS) and activity-based protein profiling (ABPP) analysis

LC-MS/MS quantification of analytes (2-AG, AA, PGD2, PGE2) was performed in the left cerebral hemisphere cerebellum of mice treated *in vivo* with MAGLi or vehicle. Healthy mice were sacrificed 24 h after the first ip injection (MAGLi 432 N = 6, vehicle N = 3) and EAE mice were sacrificed at 24dpi (N = 6 per experimental group). For *ex vivo* experiments, EAE (N = 2, n = 3 slices) and CFA (N = 2, n = 10 slices) mice were sacrificed (at 20–24 dpi) and LC-MS/MS quantification was performed on corticostriatal slices (190 μm thickness), incubated with MAGLi or vehicle, placed in 1,5 mL vials (two slices for vials) and snap frozen in dry ice. The vials were stored at −80 °C.

LC-MS/MS analysis: frozen brains or brain slices were placed into 7 mL hard tissue homogenizing vials prefilled with ceramic beads (Bertin Instruments, Cat.No. P000935-LYSK0-A.0) and homogenized in methanol using a Precellys homogenizer (Bertin Instruments, Cat.No. P000062-PEVO0-A) operating at 3 × 10s, 6000 rpm giving a final concentration of 100 mg tissue/mL methanol. Brain homogenates were purified by protein precipitation followed by centrifugation (18000 g for 10min). Aliquots of the cleaned samples were further diluted 1:2 with methanol containing internal standards prior to analysis. Undiluted

precipitates were used to measure AEA, PGE2 and PGD2 levels, whereas precipitates were diluted 1:100 to measure 2-AG and arachidonic acid (2 μL of each sample was injected). Calibration samples were prepared accordingly using cleaned aliquots of pooled brain homogenates spiked with 10-fold concentrated calibration standards serially diluted in methanol. The internal standards for arachidonic acid, 2-AG, AEA, PGE2 and PGD2 were AA-d8, 2-AG-d5, AEA-d8, PGE2-d4 or PGD2-d9, respectively (all from Cayman Chemicals, Ann Arbor, MI, USA). All calibration curves were fitted using a linear regression function with 1/y weighting, excluding zero and absolute concentrations were calculated by dividing the peak area ratio (= peak area analyte/peak area internal standard) by the slope of the calibration curve.

ABPP analysis was performed in the cerebellum of EAE mice treated *in vivo* with MAGLi or vehicle and sacrificed at 24 dpi (N = 6 per experimental group). For *ex vivo* MAGLi treatment, EAE mice were sacrificed (at 20–24 dpi, N = 2, for both MAGLi and VHL) and ABPP analysis was performed on corticostriatal slices (190 μm thickness, n = 3 for both conditions) placed in 1,5 mL vials (two slices for vials) and snap frozen in dry ice. The vials were stored at −80 °C.

ABPP analysis: cerebella (*in vivo*) and corticostriatal slices (ex-vivo) were homogenized in ABPP lysis buffer (20 mM HEPES, 2 mM DTT, 1 mM MgCl2, 0.1% Benzonase® Nuclease, ≥250 units/μL), incubated for 30 min on ice and centrifuged at 13000 rmp, for 10 min at 4 °C. The supernatants were collected and the total protein concentration was determined using Pierce 660 nm Protein Assay (ThermoFisher, cat. nr. 22,662) following the manufacturer's instruction. The total protein concentration of each sample was adjusted to 2 or 1 mg/mL with ABPP storage buffer (20 mM HEPES, 2 mM DTT). In a 96 well plate, 19.5 μL of samples were incubated with 0.5 μL 80 nM MAGL-specific fluorescent probe (Kemble et al., 2022) for 25 min at RT. The reaction was stopped by the direct addition of 12.5 μL dH2O, 12.5 μL NuPAGETM LDS Sample Buffer (4×, ThermoFisher, cat. nr. NP0007) and 5 μL NuPAGETM Sample Reducing Agent (10×, ThermoFisher, cat. nr. NP0004) followed by incubation of the plate on ice for 30 min. The samples were then separated by gel electrophoresis. 25 μL of samples were loaded in a 12% polyacrylamide gel (NuPAGETM 12% Bis-Tris, 1.0 mm, Mini Protein Gel, 10-well, cat. nr, NP341BOX) and run for 55 min at 200 V in NuPAGETM MES SDS Runnung Buffer (diluted to 1*X* in dH2O, cat. nr. NP0002). The picture acquisition was performed using the ChemiDoc system (BioRad) with Cy5 filter settings and automated acquisition time. An actin Western Blot was performed as loading control. The gels were transferred on nitrocellulose membranes using iBlotTM 2 Transfer Stacks (ThermoFisher, cat. nr. IB23001) and the iBlotTM 2 Gel Transfer Device (ThermoFisher, cat. nr. IB21001) following the manufacturer's instructions. The membranes were blocked with 5% nonfat milk in PBS-Tween 0.1% for 1 h at RT and stained with an HRP-labeled *anti*--β-actin antibody (Abcam, cat. nr ab49900) diluted 1:25000 in 5% nonfat milk,PBS-Tween 0.1%, overnight, at 4 °C while shaking. The membranes were washed three times for 5 min with PBS-Tween 0.1% and developed with SuperSignal TM West Dura Extended Duration Substrate (ThermoFisher, cat. nr. 37071) following the manufacturer's instructions. The membrane picture was taken using ChemiDoc system (BioRad), using a minimum exposure time of 1 s.

### 2.9. Statistical analysis

Statistical analysis was performed with Prism GraphPad version 9.0 and by BioRad Image Lab Software (for ABPP quantification). Data distribution was tested for normality by using Kolmogorov–Smirnov test. Non-normally distributed data were analysed through non-parametric tests. Data were presented as the mean ± S.E.M and the significance level was established at $p < 0.05$. Differences between two groups were analysed using two-tailed Paired or Unpaired Student's *t*-test, as appropriate. Multiple comparisons were performed by One-Way ANOVA followed by Tukey's HSD or Two-Way ANOVA followed by Bonferroni Post Hoc. Differences between groups in clinical score analysis were tested by Mann–Whitney test and by log-rank test. The exact statistical test used for each experiment and its details can be found in the figure legends. Throughout the text "N" refers to the number of animals. For electrophysiological experiments and quantitative immunofluorescence analysis or *ex vivo* experiment "n" refers to the number of cells recorded or slices analysed, respectively.

## 3. Results

### 3.1. In vivo treatment with MAGLi 432 ameliorates clinical score and motor performance in EAE mice

Before assessing the effect of MAGL inhibition on $MOG_{35-55}$ EAE animal model, we evaluated if MAGLi 432 administration could change eCB brain content in healthy mice. We observed a significant increase in 2-AG levels and a concomitant decrease in AA, PGE2, and PGD2 levels in C57BL/6 mice acutely treated with MAGLi 432 (2 mg/kg) compared to VHL-treated mice. Conversely, as expected by a selective inhibitor of the degradative enzyme of 2-AG, MAGLi-432 did not modulate the levels of AEA (Fig. 1A).

Then, we investigated the impact of MAGLi 432 treatment on EAE clinical course. We performed daily intraperitoneal injections of MAGLi 432 (2 mg/kg/day) or VHL starting from 0 day post immunization (0 dpi) until the acute phase of the disease (24 dpi). We observed that MAGLi 432 induced a less severe EAE disease compared to mice treated with VHL, with a significant difference emerging around 16–24 dpi (Fig. 1B).

To evaluate whether these beneficial effects were accompanied by an improvement in neuromuscular function, we assessed the maximal force of the mice using the grip strength test before the appearance of clinical deficits and during the acute phase of the disease (Fig. 1C). During the early phase of the disease (14 dpi), MAGLi 432-treated mice showed a better performance in terms of strength of both fore and hind-limb relative to the vehicle group, an effect that disappeared at 21 dpi. Body weight was similar between MAGLi and VHL mice during the entire course of the disease (Fig. 1D), indicating a negligible impact of the drug on this parameter.

ABPP biochemical analyses performed on mouse brain samples at 24 dpi demonstrated the MAGL target occupancy of MAGLi 432 (Fig. 1E). LC/MS analysis of 24 dpi brain hemisphere showed a significant increase of 2-AG levels combined with a concomitant and significant decrease of AA, PGD2 and PGE2 levels (Fig. 1F) thus confirming MAGL target engagement in the brain of the MAGLi 432 treated mice. Notably, anandamide (AEA) was not modulated by the treatment, supporting the specificity of MAGLi 432 for MAGL enzyme.

The beneficial effect of MAGLi on EAE clinical disability was confirmed in a second experimental set where a significant difference was also observed in terms of disease incidence (Supplementary Fig. 2).

### 3.2. MAGLi 432 in vivo treatment reduces striatal microgliosis and astrogliosis in EAE mice

The effect of MAGLi 432 treatment on neuroinflammation was evaluated by immunofluorescence and confocal analysis. The immunostaining of microglia/macrophages (IBA1/TMEM positive cells) and astroglia (GFAP positive cells) were performed in the striatum, a brain region highly sensitive to the neuroinflammatory and neurodegenerative processes of MS/EAE (Centonze et al., 2009; Tao et al., 2009; Haji et al., 2012) and strongly modulated by the ECS (Centonze et al., 2007b; Musella et al., 2014; Lovinger and Mathur, 2016).

Quantification of microglia/macrophages density showed a significant reduction of IBA1+ cells in EAE-MAGLi compared to EAE-VHL at 24 dpi (Fig. 2 A-A'). Such an effect was maintained during the chronic phase of the disease (35 dpi), as revealed in the second experimental set (Supplementary Fig. 3).

A main feature of microglia is its rapid morphological change upon

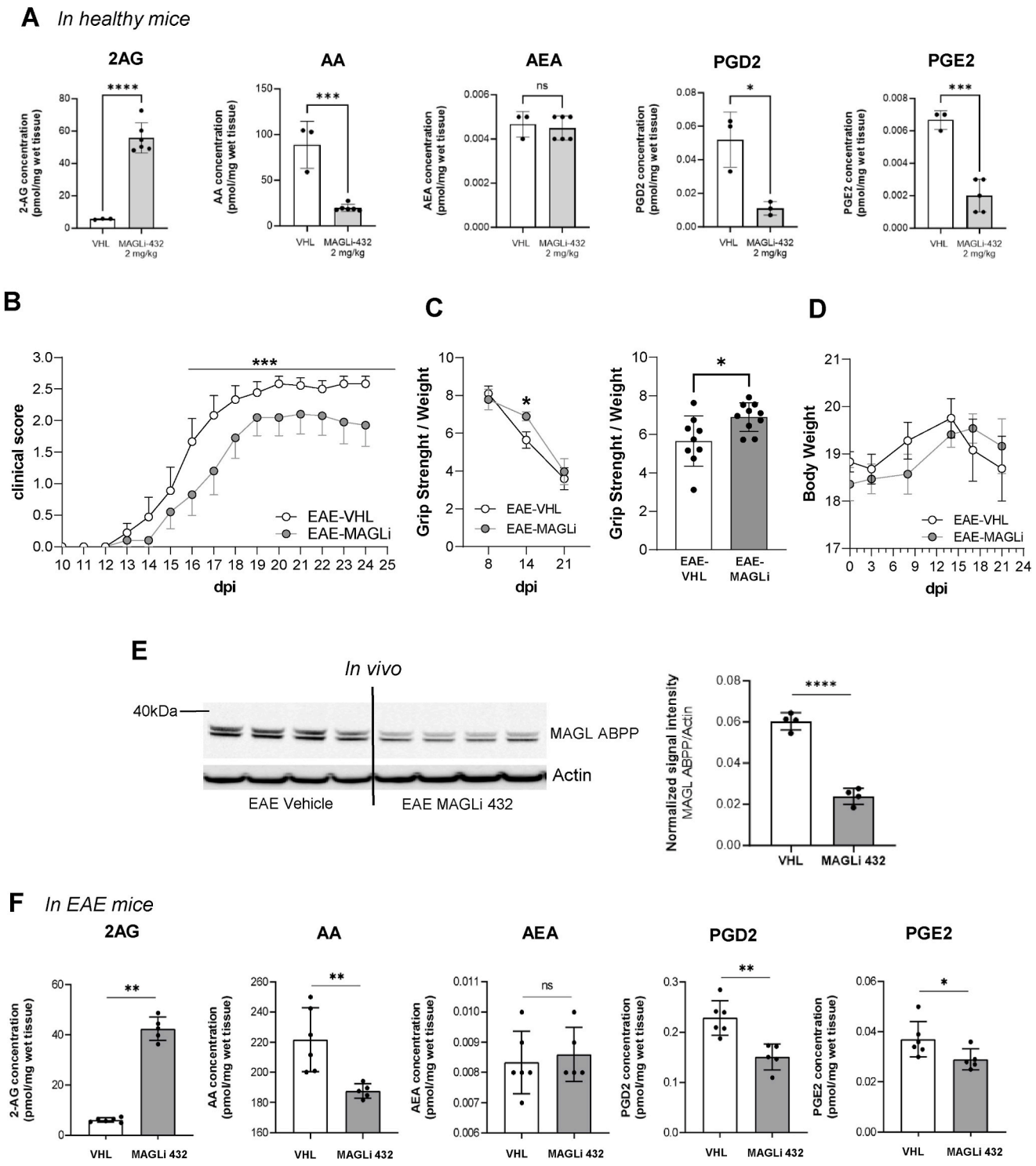


**Fig. 1.** Preventive and peripheral MAGLi 432 treatment ameliorates motor dysfunctions in EAE mice.
(A) LC/MS analysis of 2-AG,AA, PGD2 and PGE2 brain levels evaluated in healthy mice treated with MAGLi 432 (acute administration, 2 mg/kg) or vehicle ((unpaired *t*-test: 2-AG t = 8.963, df = 7 p < 0.0001; AA t = 6.887, df = 7, p = 00002; PGD2 t = 4.177, df = 4, p = 00139; PGE2 t = 7.246, df = 6 p = 0.0004). (B) The graph shows the EAE clinical course of mice treated with VHL or MAGLi 432 (MAGLi). MAGLi treatment started at 0 dpi (daily i. p. 2 mg/kg) significantly reduced motor disability between 16 and 24 dpi (EAE VHL: N = 9; EAE MAGLi N = 10; Mann Whitney test U = 2470, p = 0.0002). (C) The grip strength test performance was significantly recovered by MAGLi 432 treatment in EAE mice in the early symptomatic phase of the disease, at 14 dpi (unpaired *t*-test t = 2.597, df = 17; p = 0.0188). This effect was not evident later on at 21 dpi. (D) The graph shows the body weight of EAE mice measured at 0, 3, 8, 14, 17, and 21 dpi. (EAE VHL N = 9, EAE MAGLi N = 10, 2 way ANOVA p = 0.4835, df = 85). (E) ABPP analysis of cerebellum samples confirms MAGL target occupancy of MAGLi 432: The average signal intensities of active MAGL in cerebellum lysates were quantified by densitometric analysis as the average intensity of the total detectable MAGL (ABPP) divided by the β-actin signal (unpaired *t*-test, mean ± SD, ****p < 0.0001). (F) LC/MS analysis confirms MAGL target engagement in the brain of MAGLi 432 treated mice as indicated by 2-AG increase with concomitant AA, PGD2 and PGE2 decrease in EAE mice (unpaired *t*-test: 2-AG t = 18.79, df = 9 p < 0.0001; AA t = 3.496, df = 9, p < 0.0068; PGD2 t = 4.175, df = 9, p = 0.0024; PGE2 t = 2.223, df = 9 p = 0.0533).

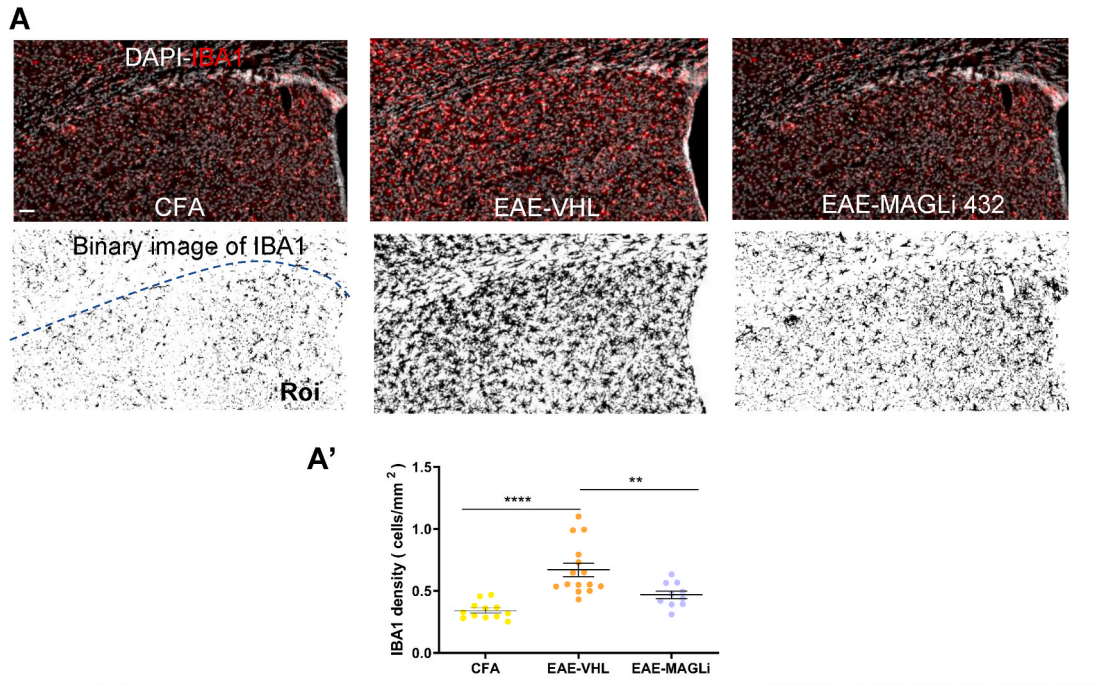





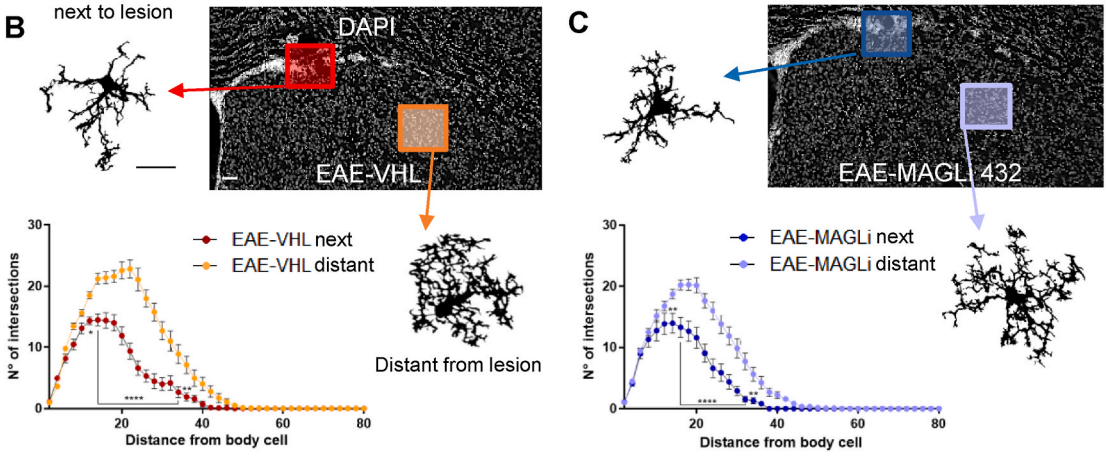


| Sholl analysis summary in EAE-VHL | | | |
|---|---|---|---|
| | next lesion | Distant lesion | Unpaired t-test |
| Ramification index | 16,07 ± 1,01 | 27 ± 1,15 | *** |
| Critical value | 15,56 ± 1,67 | 24,5 ± 1,01 | *** |
| | | | |
| Number of cells | 12 | 22 | |

| Sholl analysis summary in EAE-MAGLi 432 | | | |
|---|---|---|---|
| | next lesion | Distant lesion | Unpaired t-test |
| Ramification index | 16,23 ± 1,85 | 22,6 ± 0,64 | *** |
| Critical value | 15,8 ± 0,86 | 21,73 ± 0,88 | *** |
| | | | |
| Number of cells | 12 | 21 | |

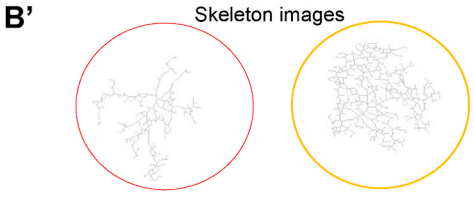


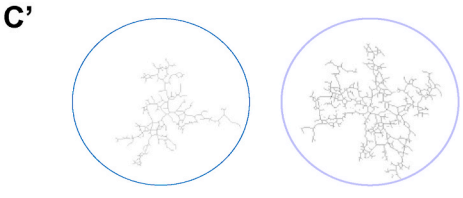


| Skeleton analysis summary in EAE-VHL | | | |
|---|---|---|---|
| | next lesion | distant lesion | Unpaired t-test |
| Number of branches | 220,42 ± 20,18 | 577,65 ± 33,64 | *** |
| Number of junctions | 115,58 ± 10,92 | 306,56 ± 17,83 | *** |
| Number of branch endpoints | 86,75 ± 7,36 | 206,83 ± 12,45 | *** |
| Avarage branch lenght (µm) | 2,14 ± 0,062 | 1,87 ± 0,02 | *** |
| Maximum branch lenght (µm) | 9,35 ± 0,47 | 10,25 ± 0,54 | ns |
| | | | |
| Number of cells | 12 | 22 | |

| Skeleton analysis summary in EAE-MAGLi 432 | | | |
|---|---|---|---|
| | next lesion | distant lesion | Unpaired t-test |
| Number of branches | 220,42 ± 26,2 | 474,62 ± 30,27 | *** |
| Number of junctions | 114,42 ± 13,85 | 251,76 ± 16,38 | *** |
| Number of branch endpoints | 89 ± 9,26 | 169,62 ± 9,59 | *** |
| Avarage branch lenght (µm) | 2,04 ± 0,057 | 1,86 ± 0,03 | * |
| Maximum branch lenght (µm) | 9,37 ± 0,45 | 8,90 ± 0,38 | ns |
| | | | |
| Number of cells | 12 | 21 | |

(caption on next page)

**Fig. 2.** Reduction of striatal microglia/macrophages density in EAE MAGLi mice and characterization of EAE striatal microglia morphology.
(A) Representative confocal microscopy images of corticostriatal slices stained with IBA1 antibody (red) and DAPI (gray) showing microglia/macrophages in all experimental groups (EAE and CFA mice) during the acute phase of the disease (24 dpi). Binary images highlighting the reduction of IBA1 cells in MAGLi treated mice (20× objective; scale bar 40 μm). (A′) The relative quantification of the IBA1+ cell density evaluated in the region of interest (roi) (one-way-ANOVA $f = 17.05$, $df = 36$ $p < 0.0001$; Tukey Post-Hoc: CFA vs EAE-VHL $p < 0.0001$, EAE-VHL vs EAE-MAGLi $p = 0.0057$; CFA $n = 12$ ($N = 4$); EAE VHL $n = 15$ ($N = 4$); EAE MAGLi $n = 10$ ($N = 3$). (B–C) Representative confocal microscopy images of EAE-VHL and EAE-MAGLi corticostriatal slices stained with DAPI (gray) showing the two different regions, next (red and blue) and distant (orange a purple) from the lesion site, where the morphological analyses were carried out (20× objective; scale bar 40 μm. Isolated microglia: 60× objective, scale bar 20 μm). The Sholl intersection profile is obtained by counting the number of microglia ramifications at a given distance from the soma; on the bottom, graphs and tables relative to the main parameters of Sholl analysis show a higher ramification rate in microglia cells distant from the lesion site in both experimental groups (two-way ANOVA, Bonferroni Post-Hoc, number of intersections: B: $f = 11.94$, $df = 39$; $p < 0.0001$; C: $f = 7.400$, $df = 39$; $p < 0.0001$).
Skeleton analysis summary in cells next and distant from the lesion site in EAE-VHL and EAE-MAGLi mice. The number of branches, junctions, end-points, the average branch length and maximum branch length is reported with relative statistical significance. On the top, Skeleton representative images of microglia derived from each experimental condition.

activation, characterized by gradual acquisition of an ameboid shape resulting in a complex multistage and multifaced activation process. Thus, by means of Sholl and Skeleton analyses, we carried out a detailed analysis of microglia branching ramification in the dorsal striatum, considering defined brain regions distant or close to the inflammatory lesion site. Lesion sites were defined by an increased cellularity denoted by the nuclear stain DAPI at the levels of the corpus callosum (CC) and dorsal striatum (DS) (Mangiardi et al., 2011). Double immunostaining for TMEM119/IBA1 was performed to distinguish infiltrating macrophages from resident microglia close to the lesion site (Amici et al., 2017) (Supplementary Fig. 4). Interestingly, we showed that the ramification rate of EAE microglia was significantly decreased next to the lesion compared to cells distant from this site, revealing for the first time a region-dependent microglial phenotype within the EAE striatum (Fig. 2B-B′ EAE-VHL; 2C–C' EAE-MAGLi and relative tables). Only the maximum branch length parameter was unchanged.

To better define the microglia activation state in the selected region distant from the lesion site, we compared the Sholl analysis between EAE and CFA microglia. The number of intersections, the ramification index, and the critical value (radius of highest count of intersection), were increased in EAE striatum compared to CFA condition, indicating a hyper-ramified intermediate phenotype of EAE microglia (Augusto-Oliveira et al., 2022) (Fig. 3A and see table in Fig. 3A'; Supplementary Fig. 5). Interestingly, the hyper-ramified activated microglia phenotype was significantly attenuated in EAE MAGLi treated animals (Fig. 3A and see table in Fig. 3A'; Supplementary Fig. 5), corroborating the anti-inflammatory effect of the drug previously described.

The skeleton analysis also showed that the number of branches, junctions and end-points of microglia were increased in EAE compared to CFA mice, revealing an elevated branching density and complexity of EAE microglia. Notably, in accordance with previous results, MAGLi 432 attenuated EAE microgliosis (see table in Fig. 3B). Moreover, the maximum branch length or average branch length of microglia were reduced in EAE-VHL compared to CFA mice, whereas both parameters were unaffected by MAGLi treatment (see table in Fig. 3B). Furthermore, we detected a hypertrophic change of microglia cell bodies following EAE induction. As shown in Fig. 3, the mean cell body area was increased in the EAE group compared to CFA mice, and significantly reduced in EAE-MAGLi group (Fig. 3 C). Regarding the analysis of microglia morphology in the region next to the lesion site, we did not detect any difference between EAE-VHL and EAE-MAGLi mice, in terms of number of intersections (Fig. 4A), ramification index and critical value (see table in Fig. 4A'). Skeleton analysis parameters were also unaffected by the treatment (Fig. 4B).

Finally, by performing GFAP immunostaining, we investigated for the first time the effect of MAGLi treatment on striatal astrogliosis, an event markedly associated with EAE induction (Grasselli et al., 2013) (Fig. 5A and Supplementary Fig. 6). Since the morphology of astroglia cells and their spread on EAE striatum can misrepresent the analysis of GFAP + cell density, we evaluated astrogliosis by measuring the percentage of astroglia area. High magnification and binary images showed a significant attenuation of astrogliosis in the striatum and corpus callosum of EAE MAGLi mice compared to EAE-VHL mice (Fig. 5B).

### 3.3. MAGLi 432 in vivo treatment reduces immune cell recruitment into CNS

MS disease is characterized by inflammatory infiltration of the CNS and, among infiltrating immune cells, autoreactive T cells initiate CNS demyelinating lesions and, likely, microglial activation and inflammatory synaptopathy (Dendrou et al., 2015; Gentile et al., 2020). To evaluate whether MAGLi treatment could reduce effectively infiltration and/or favor resolution of inflammation, we isolated immune cells infiltrating the brain and spinal cord of EAE VHL and MAGLi treated mice. By means of flow cytometry, we quantified and defined the populations of infiltrates in the acute phase of the disease (Fig. 6A). We observed a reduced number of all nucleated hematopoietic cells ($CD45^+$ cells, unpaired *t*-test $p < 0.05$) as well as T cells ($CD3^+$ cells) in the CNS of EAE MAGLi animals compared to VHL mice. Within $CD3^+$ cells, we noticed a decreasing trend, although not significant, of both CD4 and CD8 sub-populations. On the other hand, no effects were observed on B cells and macrophages. Flow-cytometry experiment was corroborated by qualitative immunofluorescence analyses of $CD3^+$ infiltrating lymphocytes in lesion sites of the corpus callosum/dorsal striatum of EAE MAGLi mice (Fig. 6 B–B′). The inflammatory lesion area was defined by nuclear DAPI staining (Mangiardi et al., 2011) and by anti-Collagen IV staining to visualize capillary walls. Co-staining of CD3 and Collagen IV suggests that the infiltration of $CD3^+$ T cells, typically enhanced in EAE brain/spinal cord lesion sites, was reduced in EAE MAGLi mice compared to EAE VHL mice, especially nearby and within capillaries (Fig. 6 B–B').

### 3.4. In vivo MAGLi 432 treatment ameliorates glutamatergic alterations in the EAE striatum

Based on the complex interaction between neuroinflammation and ECS in modulating EAE synaptopathy, we investigated a potential beneficial effect of MAGLi 432 treatment on EAE synaptic dysfunction. To this aim, we performed whole-cell voltage-clamp recordings from medium spiny neurons (MSNs) to evaluate both spontaneous glutamatergic (sEPSCs) (20–24 dpi) and GABAergic (sIPSCs) transmission (30–34 dpi) of EAE mice *in vivo* treated with MAGLi or VHL.

Remarkably, daily systemic treatment with MAGLi ameliorated glutamatergic alterations that characterizes the EAE striatum. Indeed, EAE treated mice showed values of sEPSC frequency similar to healthy mice and significantly different compared to EAE VHL mice (Fig. 7A) whereas the sEPSC kinetics were not affected (Supplementary Fig. 7). The frequency and amplitude of the EAE GABAergic transmission were not affected by the treatment (Supplementary Fig. 7). Furthermore, we investigated the involvement of CB1 receptors, whose activation is known to mediate a tonic suppression of glutamatergic transmission. However, as shown in Fig. 7B, incubation of AM281, a potent and

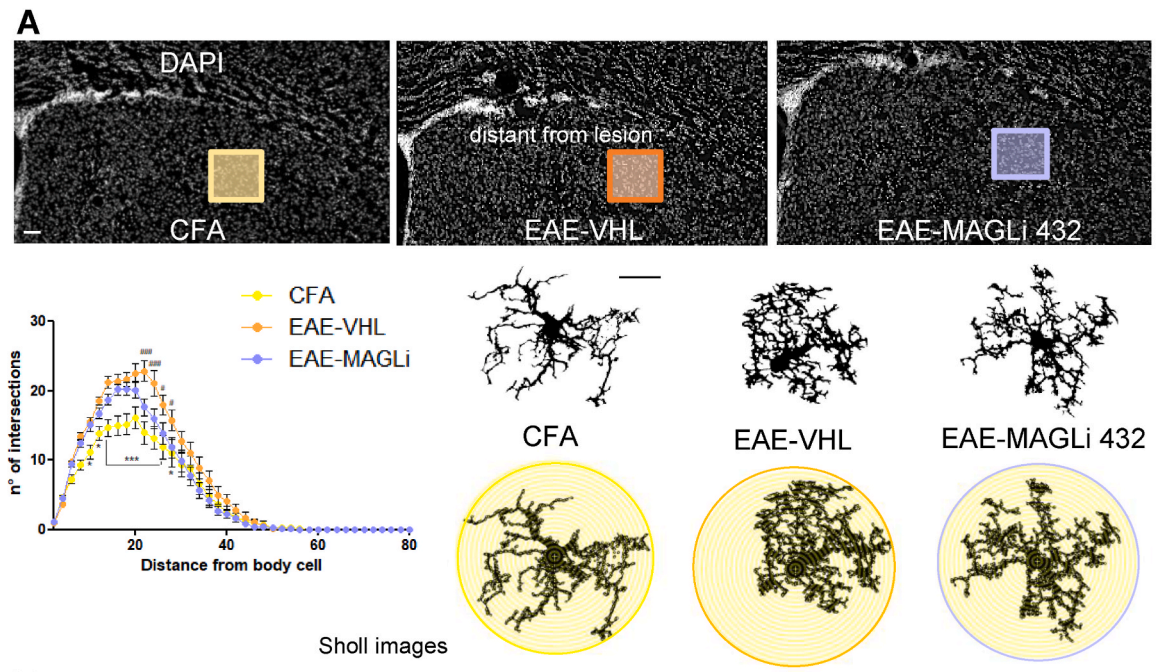


A'

| Sholl analysis summary (* One Way ANOVA, Tukey Post-Hoc ) | | | | | | |
|---|---|---|---|---|---|---|
| | CFA | EAE-VHL | EAE-MAGLi | CFA vs EAE-VH | CFA vs EAE-MAGLi | EAE-VH vs EAE-MAGLi |
| Ramification index | 18,18 ± 1,79 | 27 ± 1,15 | 22,6 ± 0,64 | *** | * | * |
| Critical Value | 16,98 ± 1,14 | 24,5 ± 1,01 | 21,73 ± 0,88 | *** | ** | t-test 0,04 |
| | | | | | | |
| Number of cells | 14 | 22 | 21 | | | |

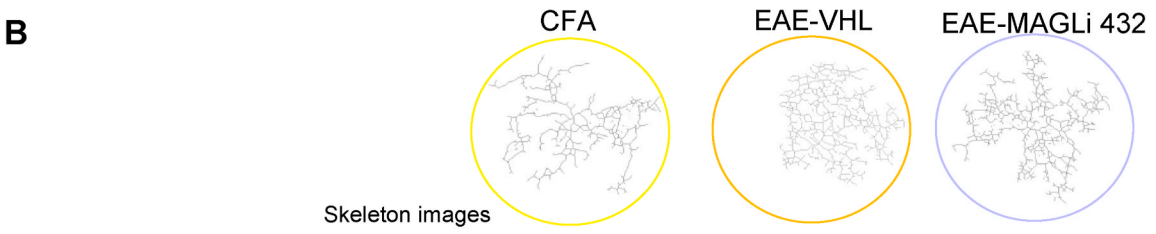


| Skeleton analysis summary (* One Way ANOVA, Tukey Post-Hoc ) | | | | | | |
|---|---|---|---|---|---|---|
| | CFA | EAE-VHL | EAE-MAGLi | CFA vs EAE-VH | CFA vs EAE-MAGLi | EAE-VH vs EAE-MAGLi |
| Number of branches | 303,71 ± 40,14 | 577,65 ± 33,64 | 474,62 ± 30,27 | *** | ** | t-test 0,03 |
| Number of junctions | 157,00 ± 20,98 | 306,56 ± 17,83 | 251,76 ± 16,38 | *** | * | t-test 0,02 |
| Number of branch endpoints | 120,71 ± 16,73 | 206,83 ± 12,45 | 169,62 ± 9,59 | *** | ** | t-test 0,03 |
| Avarage branch lenght (µm) | 2,17 ± 0,09 | 1,87 ± 0,02 | 1,86 ± 0,03 | ** | *** | ns |
| Maximum branch lenght (µm) | 13,35 ± 0,98 | 10,25 ± 0,54 | 8,90 ± 0,38 | *** | *** | ns |
| | | | | | | |
| Number of cells | 14 | 22 | 21 | | | |

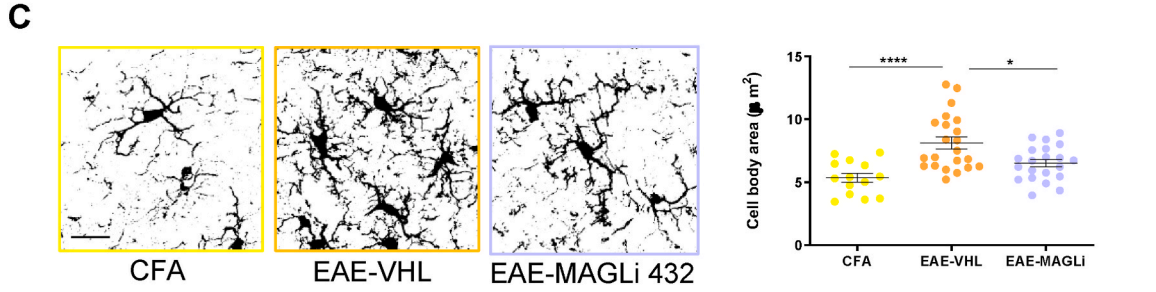


*(caption on next page)*

**Fig. 3.** MAGLi 432 *in vivo* treatment impacts on microglia morphology in EAE striatum distant from the lesion site.
(A) Representative confocal microscopy images of corticostriatal slices stained with DAPI (gray) showing the region (distant from the lesion site) where the morphological analyses were carried out in all experimental groups (EAE and CFA mice) (20× objective; scale bar 40 μm; isolated microglia: 60× objective; scale bar 20 μm). EAE mice have an increased ramification of the microglia harbor compared to CFA mice and MAGLi 432 treatment significantly reduced the number of intersections (two-way ANOVA, interaction: $f = 4.401$, $df = 39$, $p < 0.001$, Bonferroni Post-Hoc).
On the right, IBA-1 binary images representative of microglia performed to generate Sholl images. (A′) Table summary of other main parameters of the Sholl analysis: ramification index and critical value. (B) Skeleton analysis summary in cells distant from the lesion site in CFA, EAE-VHL and EAE-MAGLi mice. The number of branches, junctions, end-points, the average branch length and maximum branch length is reported with relative statistical significance. On the top, Skeleton represents images of microglia. *CFA vs EAE-VHL, #:EAE-VHL vs EAE-MAGLi: (C) Analysis of cell body area shows an increase in EAE-VHL mice compared to CFA mice and a reduction in EAE-MAGLi animals (60× objective; scale bar 20 μm) (one-way-ANOVA: $f = 11.38$, $df = 56$, $p < 0.0001$; Tukey Post-Hoc: CFA vs EAE-VHL $p < 0.0001$, EAE-VHL vs EAE-MAGLi $p = 0.0104$; CFA $n = 14$ ($N = 3$); EAE VHL $n = 22$ ($N = 3$); EAE MAGLi $n = 21$ ($N = 3$).

selective CB1 antagonist, did not affect sEPSC frequency of EAE-MAGLi slices suggesting a chronic, rather than tonic, effect of the treatment. Notably, *in vivo* treatment with MAGLi in healthy mice did not change synaptic properties of glutamatergic events, in terms of frequency and response to AM281, suggesting a specific synaptic effect of the drug during pathological condition (Fig. 7C).

### 3.5. Activation of CB1 receptor promoted by MAGLi 432 rescues EAE striatal glutamatergic alterations

To explore a possible direct effect of MAGLi on EAE striatal synaptic transmission, we performed *ex vivo* experiments by incubating corticostriatal slices derived from EAE mice (20–24 dpi; $n = 6$) for 1-h with MAGLi 432 (1 μM) or VHL directly. Acute MAGL inhibition resulted in complete MAGL target occupancy, as demonstrated by ABPP (Fig. 8A), and induced a significant modulation of 2-AG and AA levels (Fig. 8B), consistent with the findings observed in the *in vivo* experiments. In parallel, *ex vivo* treatment with MAGLi 432 in EAE slices completely rescued the exacerbation of EAE glutamatergic frequency (Fig. 8C). Such an effect was abolished by concomitant incubation with AM281 (2 μM) the CB1 antagonist, suggesting a direct involvement of CB1 receptor in this acute MAGLi-mediated synaptic modulation.

## 4. Discussion

In the present study, we investigated the neuroprotective effects of a selective and reversible MAGL inhibitor on EAE disease, uncovering for the first time a relevant impact of 2-AG metabolism on inflammatory-mediated synaptopathy. We demonstrated that daily peripheral administration of MAGLi 432 ameliorates EAE clinical disability, counteracted striatal synaptic dysfunction and neuroinflammation. Indeed, MAGLi treated EAE mice showed less infiltration of T lymphocytes in the CNS and microglia/astroglia activation. The reduction of the inflammatory status together with a CB1-dependent suppression of glutamatergic transmission could account for the amelioration of striatal synaptopathy and clinical disability.

The efficacy of the pharmacological treatment was confirmed by increased brain levels of 2-AG and reduced prostaglandin synthesis. The enhancement of 2-AG promoted by the inhibition of MAGL enzyme could induce different interconnected mechanisms that underlie the beneficial effects here observed: the endogenous stimulation of both CB1 and CB2, and the reduction of eicosanoid production. Indeed, 2-AG is a full agonist of both CB receptors, and acid arachidonic (AA), its main metabolite, is the precursor of pro-inflammatory prostaglandins (PGs) (Nomura et al., 2008, 2011). Within the CNS, 2-AG could exert both neuroprotective and anti-inflammatory effects. CB1 is expressed by glial cells (oligodendrocytes, astrocytes, macrophages/microglia), pericytes and endothelial cells, although the most important location for this receptor is neuronal (Zou and Kumar, 2018). Indeed, eCBs primarily regulate synaptic function by suppressing neurotransmitter release acting on the presynaptic terminal at excitatory and inhibitory synapses (Castillo et al., 2012). CB2 is expressed only by a few neuronal populations (Stella, 2010; Kendall and Yudowski, 2017) while it is expressed by cells of the immune system (e.g. B and T lymphocytes) and endothelial cells. Noteworthy, CB2 is abundantly expressed by activated astrocytes and microglia (Stella, 2010; Kendall and Yudowski, 2017). In the last years, the regulation of microglia M2 polarization mediated by eCBs has been described (Tanaka et al., 2020), including the reduction of microglial proinflammatory cytokine release (Ehrhart et al., 2005; Ma et al., 2015) and the modulation of microglial phagocytic function (Ehrhart et al., 2005). Moreover, a role for cannabinoids in the modulation of astrocytic response was also pointed out, particularly through mechanisms involving AEA and palmitoylethanolamide (PEA). Importantly, astrocytes have a well-recognized role on eCB degradation and astrocytic-specific deletion of MAGL was shown to attenuate neuroinflammation (Eraso-Pichot et al., 2023). MS is characterized by massive CNS inflammatory infiltrates comprising an intricate coordination of the innate and adaptive immune systems. Notably, histopathology of post-mortem tissue derived from MS patients showed CB receptor expression in infiltrated T-lymphocytes and revealed CB2-immunoreactive microglia/macrophages in MS lesions (Yiangou et al., 2006).

Our data demonstrate that MAGLi 432 modulates inflammatory response in EAE brain. The increased 2-AG tone and the decreased AA levels could attenuate neuroinflammation by different mechanisms that include: i) an immunoregulatory action on T cells and monocytes ii) a modulation of the blood-brain barrier (BBB) permeability targeting endothelial cells (Piro et al., 2018) iii) a direct interplay with microglia and astroglia cells. Our data from flow cytometry data suggest that monocyte activation and infiltration were not affected by MAGLi 432 treatment in EAE mice. Moreover, in a different neuroinflammatory condition and under a different pharmacological regimen, it was recently shown that MAGLi 432 did not ameliorate lipopolysaccharide-induced blood–brain barrier permeability (Kemble et al., 2022). Conversely, Piro and colleagues observed that a different MAGL inhibitor, CPD-4645, reduced BBB permeability in both LPS-challenged and ischemic inflammatory injured mice, partially through CB1 and CB2 signaling (Piro et al., 2018). Based on these observations, we can speculate that, in our condition, MAGLi 432 triggers events that could counterbalance neuroinflammation by modulating peripheral T lymphocytes infiltration and/or by directly mitigating astrogliosis and microgliosis. Evidence suggests cannabinoids as critical players in promoting a reparative state of microglia in EAE, however the precise mechanisms underlying this effect need to be further defined (Tanaka et al., 2020; Duffy et al., 2021). Cannabinoid agonists have been shown to reduce the clinical severity of murine models of EAE and were associated with decreased microglia/macrophage activation in the CNS (Kozela et al., 2011; Carrillo-Salinas et al., 2014; Rahimi et al., 2015). Alongside their effect on reducing microglia/macrophage activation and clinical severity, synthetic CB2-selective agonists have also been shown to attenuate T cell infiltration, oxidative damage and axonal loss in the spinal cord of EAE mice, as well as to mitigate microgliosis and astrogliosis in the corpus callosum of cuprizone mice, thus accelerating remyelination process (Alberti et al., 2017; Navarrete et al., 2020). Interestingly, de Lago et al. (De Lago et al., 2012) have shown that the beneficial effects of cannabinoid-based therapies on EAE severity and microglial/macrophage activation in the CNS appear to be mediated through CB1 receptors (De Lago et al., 2012). In support of this finding,

A

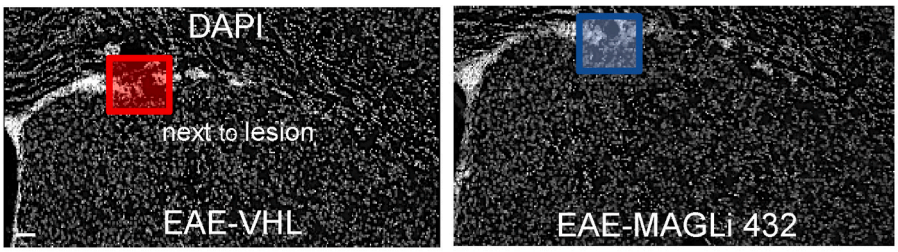


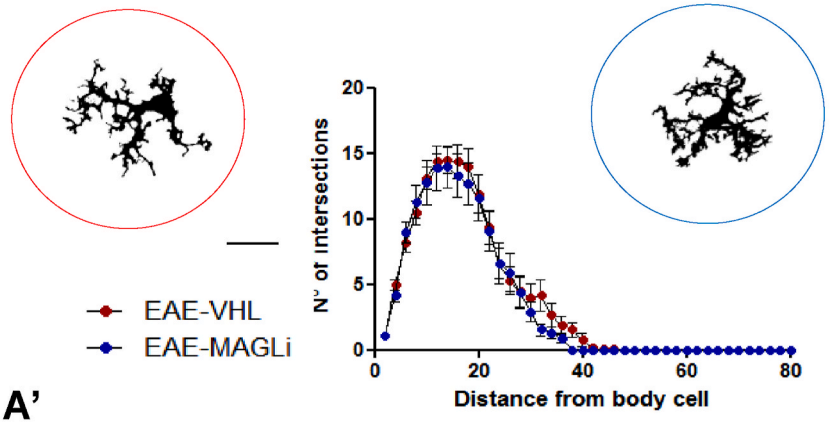


A'

| Sholl analysis summary | | | |
|---|---|---|---|
| | EAE-VHL | EAE-MAGLi 432 | Unpaired t-test |
| Ramification index | 16,07 ± 1,01 | 16,23 ± 1,85 | ns |
| Critical value | 15,56 ± 1,67 | 15,8 ± 0,86 | ns |
| | | | |
| Number of cells | 12 | 12 | |

Skeleton images

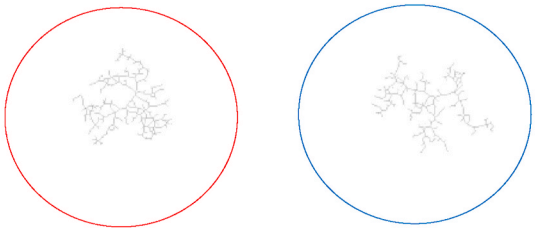

B

| Skeleton analysis summary | | | |
|---|---|---|---|
| | EAE-VHL | EAE-MAGLi | Unpaired t-test |
| Number of branches | 220,42 ± 20,18 | 220,42 ± 26,2 | ns |
| Number of junctions | 115,58 ± 10,92 | 114,42 ± 13,85 | ns |
| Number of branch endpoints | 86,75 ± 7,36 | 89 ± 9,26 | ns |
| Avarage branch lenght (μm) | 2,14 ± 0,062 | 2,04 ± 0,057 | ns |
| Maximum branch lenght (μm) | 9,35 ± 0,47 | 9,37 ± 0,45 | ns |
| | | | |
| Number of cells | 12 | 12 | |

**Fig. 4.** MAGLi 432 *in vivo* treatment does not affect microglia morphology in EAE striatum next to the lesion site.
(A) Representative confocal microscopy images of corticostriatal slices stained with DAPI (gray) showing the region (next to the lesion site) where the morphological analyses were carried out both in EAE-VHL and EAE-MAGLi mice (20× objective; scale bar 40 μm; isolated microglia: 60× objective, scale bar 20 μm). Sholl graph (A) and relative table (A') show no difference regarding the number of microglia intersections and ramification index and critical value between the two experimental groups. (B) Skeleton parameters are not affected in microglia following MAGLi 432 treatment.

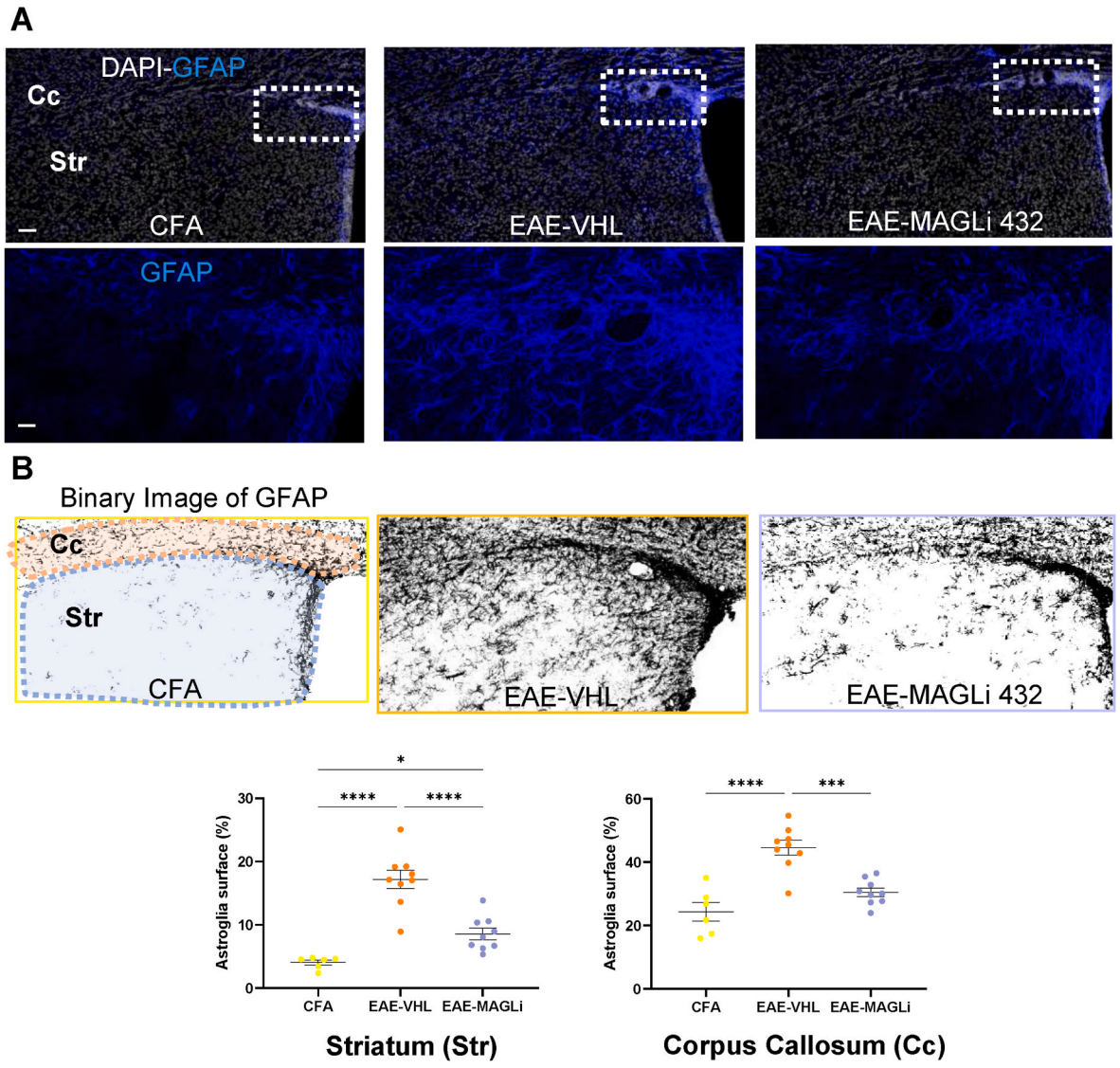


**Fig. 5.** MAGLi 432 treatment reduces astrogliosis in EAE striatum.
(A) Representative confocal images of corticostriatal slices immunostained with GFAP antibody (blue) and DAPI (gray) show an attenuation of astroglia activation. The percentage of the area occupied by astroglia is reduced in EAE-MAGLi mice compared to EAE-VHL mice in dorsal striatum (str) (one-way ANOVA: $f = 31.17$, $df = 32$, $p < 0.0001$; Tukey Post-Hoc: CFA vs EAE-VHL $p < 0.0001$, EAE-VHL vs EAE-MAGLi $p = 0.0002$, CFA vs EAE-MAGLi $p = 0.0444$; and corpus callosum (cc) (one-way ANOVA: $f = 15.86$, $df = 32$, $p < 0.0001$; Tukey Post-Hoc: CFA vs EAE-VHL $p < 0.0001$, EAE-VHL vs EAE-MAGLi $p = 0.0002$; CFA $n = 11$ ($N = 4$); EAE VHL $n = 15$ ($N = 4$); EAE MAGLi $n = 11$ ($N = 3$). The bottom panel is a high magnification of the white insets, highlighting an attenuation of GFAP staining in the lesion sites of MAGLi treated mice (20× objective; Scale bars 40 μm and 20 μm). (B) Binary images clearly highlight the MAGLi 432 effect on astrogliosis.

treatment of EAE mice with the synthetic cannabinoid CB52 alleviates clinical disease and reduces spinal cord microglia activation, T cell infiltration and damage. These effects were mediated by the activation of CB1 receptors (Ribeiro et al., 2013).

In the present study, the detailed analysis of microglia morphology describes for the first time the complex changes of microglia phenotype in EAE striatum and highlights the impact of MAGLi on these processes. Microglia and infiltrating macrophages are known to participate in both beneficial and detrimental processes during MS development, and this dichotomic behavior could be explained by different activation states of these cells (Montilla et al., 2023). This complex and rapid cellular process includes changes in cell numbers and cellular morphology resulting in a context- and time-dependent signature of microglia cells. For these reasons, microglia morphology modifications cannot be simply described as a transition from ramified to ameboid shape. Our results showed that in the EAE striatum, the region distant from the inflammatory lesion site, is characterized by hyper-ramified microglia with an intermediate activation state characterized by a "bushy-like" appearance (Morrison et al., 2017; Augusto-Oliveira et al., 2022; Vidal-Itriago et al., 2022). On the other hand, next to the lesion site, EAE microglia reduced their ramification rate displaying transition into ameboid morphology. Of note, MAGLi 432 treatment counteracted microglia activation state by reducing striatal cell density and modulating cellular morphological phenotype. In particular, the drug effect on morphological activation was mainly appreciable in cells distant from the lesion site where, probably, brain damage is not exacerbated and where, importantly, electrophysiological recordings were performed.

Together with microglia, astrocytes play a key role in EAE neuroinflammation and respond to brain damage by upregulating GFAP expression which is used as a marker for astrogliosis. This activation process is associated with functional, morphological and biochemical changes (Aharoni et al., 2021). While some data described the effect of MAGLi on microglia, very few data exist on MAGLi and reactive astrocytes. Here, we observed for the first time that MAGLi treatment

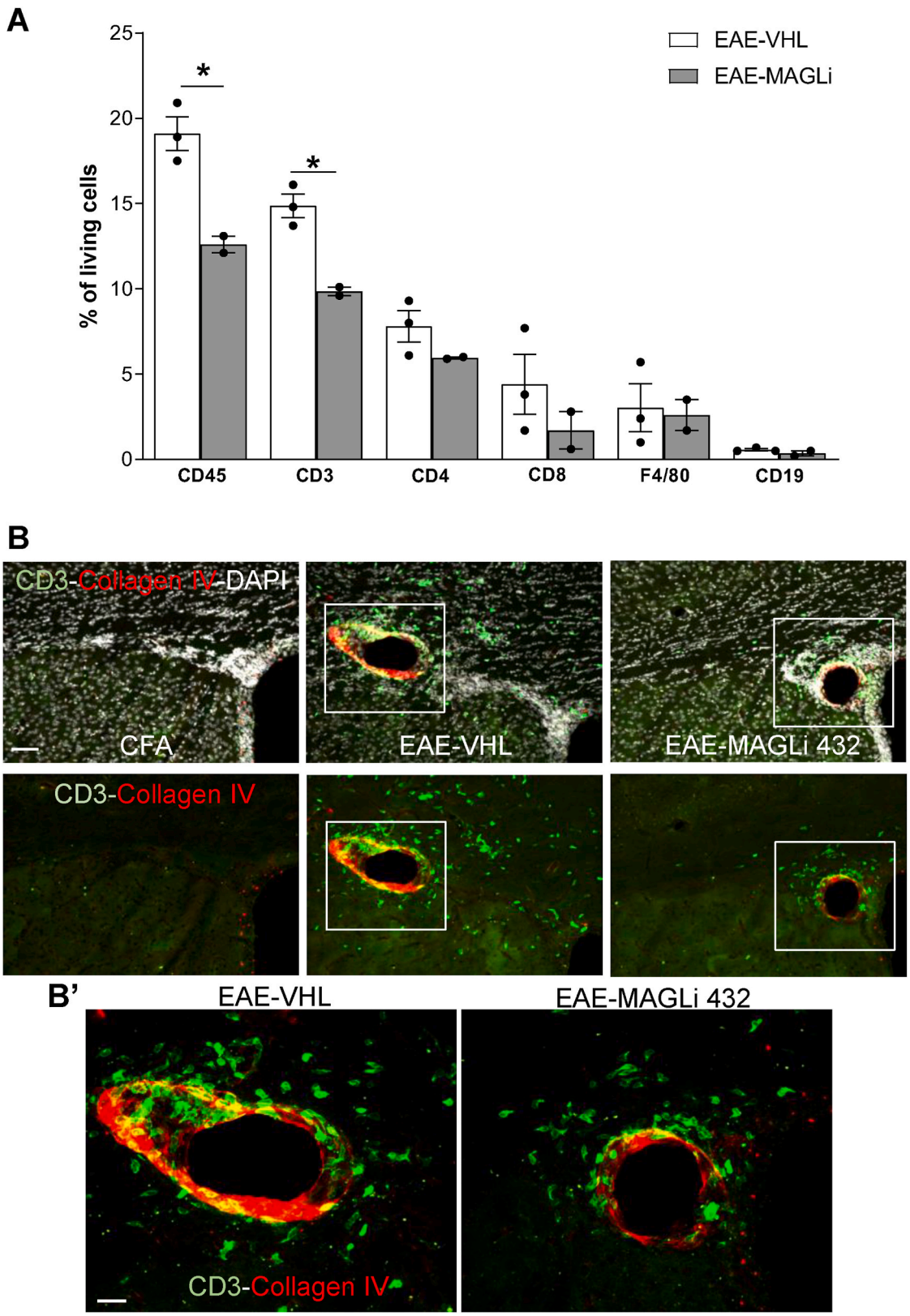


**Fig. 6.** MAGLi 432 *in vivo* treatment reduces infiltrating lymphocytes.
(A) The histogram shows the percentage of CD45, CD3, CD4, CD8, F4/80 and CD19 in gated living cells into the CNS (brain and spinal cord) of EAE-VHL and EAE MAGLi 432 mice (21–23 dpi). MAGLi 432 treatment significantly reduced the percentage of CD45 (unpaired *t*-test t = 4,898, df = 3; p = 0.0163) and CD3 cells (unpaired *t*-test t = 5485 df = 3; p = 0.00119) (EAE-VHL: n = 3 (from 12 mice), EAE-MAGLi: n = 2 (from 8 mice). (B) Representative confocal microscopy images of corticostriatal sections from CFA, EAE-VHL and EAE MAGLi 432 mice (21 dpi) show the presence of inflammatory lesions (red), detected by collagen IV positive brain microvessels, and the infiltration of $CD3^{+}$ T cells (green) (20× objective, scale bar 40 μm). (B′) On the bottom, high magnification images showing lymphocytes nearby and within microvessels. Nuclei are counterstained with DAPI (40× objective, scale bar 20 μm).

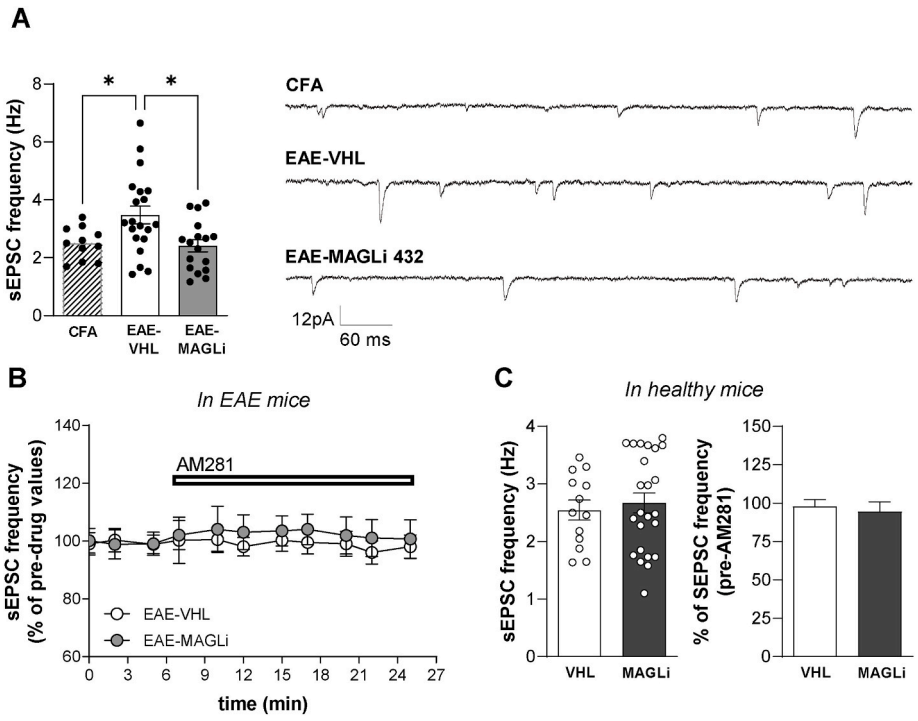


**Fig. 7.** Effects of *in vivo* MAGLi 432 treatment on striatal glutamatergic transmission.
(A-B) Whole-cell patch clamp recordings of MSNs from EAE corticostriatal slices show the effects of MAGLi 432 *in vivo* treatment on the spontaneous postsynaptic glutamatergic current (sEPSC) (A) The histogram reports a significant reduction of sEPSC frequency recorded from EAE-MAGLi mice in comparison to EAE-VHL, indicating a recovery to healthy condition (CFA) (one-way ANOVA: f = 5.419, df = 45, p = 0.0078, Tukey Post-Hoc: EAE-VHL vs EAE-MAGLi 0.0117, EAE-VHL vs CFA p = 0.0485; EAE-VHL: n = 20; EAE-MAGLi n = 17; CFA n = 11). On the right, examples of electrophysiological traces of the three experimental groups. (B–C) Electrophysiological data show that the perfusion with the CB1 antagonist AM281 (2 μm) did not alter sEPSC frequency compared to the pre-drug condition in EAE-MAGli and EAE-VHL animals, both during EAE condition (B) and in healthy mice (C).

promotes a strong attenuation of astroglia activation in EAE striatum, thus contributing to the resolution of neuroinflammation.

In parallel, the pharmacological treatment with MAGLi 432 counterbalanced the aberrant glutamatergic transmission that characterizes EAE striatum by recovering glutamate-mediated sEPSC frequency. The reduction of the inflammatory status and glutamatergic transmission could account for the amelioration of the clinical score and grip strength. The disappearance of the beneficial effect of MAGLi 432 on grip strength at 21 dpi could potentially be attributed to selective CB1 desensitization in specific cells/circuits involved in this behavior (Bouchet et al., 2023). Notably, glutamatergic and GABAergic synapses are privileged sites of action for eCBs that act in concert with proinflammatory cytokines (Rossi et al., 2014; Chiurchiù et al., 2018). Activation of CB1 reduces the frequency of spontaneous glutamate-mediated synaptic currents in striatal neurons, thus contrasting the effects of IL-1β on glutamate release from presynaptic nerve terminals (Musella et al., 2014). eCBs are generally synthesized "on demand" and can suppress transmitter release in a transient (short-) or long-lasting manner (Castillo et al., 2012). Importantly, neuroinflammation promotes synaptic dysfunction in EAE striatum and the anti-inflammatory effect mediated by MAGLi 432 could support the modulation of glutamate transmission. Thus, the anti-inflammatory effect combined with the direct CB1-dependent suppression of neurotransmitter release could account for the anti-synaptotoxic effect observed during MAGLi 432 treatment. Of note, acute application of CB1 antagonist (AM281) after a long-lasting- treatment with MAGLi 432 did not change glutamate frequency. This result could be ascribed to a consolidated process of reduced presynaptic glutamate release. However, we can not exclude the possibility that the lack of AM281 effect is influenced by adaptation/desensitization of the CB receptors induced by a chronic stimulation (Bouchet et al., 2023). Conversely, concomitant bath application of MAGLi 432 and CB1 antagonist, abolished the acute effect of MAGLi on sEPSCs, confirming that inhibition of the degradative enzyme of 2-AG promotes the stimulation of CB1 presynaptic receptors.

Noteworthy the significance of the pharmacological approach used in this study relies on the fact that the reversible inhibition of MAGL has the capacity to increase the 2-AG tone avoiding strong side effects associated with direct CB agonist (Tuccinardi et al., 2014).

## 5. Conclusions

Disease course and progression of MS are heterogeneous and the impact of ECS on CNS homeostasis is equally disparate. This study provides valuable insights into the role of MAGL inhibition in MS. Notably, several clinical trials are ongoing with MAGL inhibitors, such as ABX-1431, which is entering clinical phase 2 studies for neurological disorders including MS. Our study sheds light on broad beneficial anti-inflammatory effects of MAGL inhibition on EAE disease thus supporting the potential efficacy of MAGL inhibitor-based therapy in MS disease.

## Ethics approval and consent to participate

Animals experiments followed the guidelines of Animal Research Reporting In Vivo Experiments (ARRIVE and were carried out according to the Internal Institutional Review Committee, the European Directive 2010/63/EU, the European Recommendations 526/2007 and the Italian D. Lgs 26/2014 (Prot. n°337/2021-PR).

## Consent for publication

Not applicable.

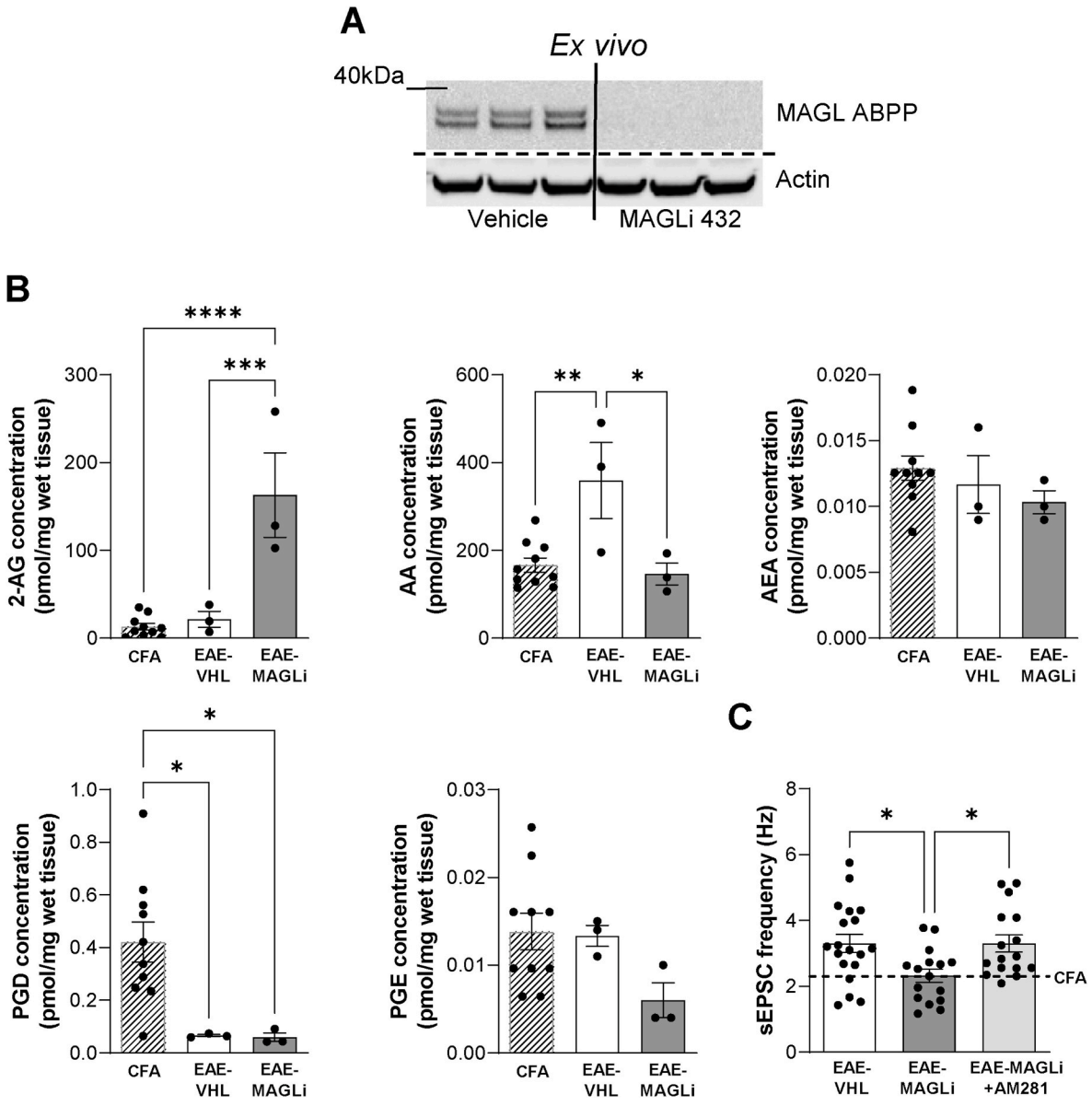


**Fig. 8.** *Ex vivo* MAGLi 432 treatment significantly modulates 2 AG brain levels and rescues striatal glutamatergic neurotransmission
(A) ABPP analysis of corticostriatal slices treated with MAGLi 432 confirms MAGL target occupancy of 2 AG. (B) LC/MS analysis of corticostriatal slices treated with MAGLi 432 modulation of 2 AG and AA levels (one-way ANOVA: f = 22.24, df = 22.24, p < 0,0001; Tukey Post-Hoc, 2 AG: EAE-VHL vs EAE-MAGLi p = 0.0007, CFA vs EAE-MAGLi p < 0.0001; AA: EAE-VHL vs EAE-MAGLi p = 0.0102, CFA vs EAE-VHL p = 0.0046). (C) Whole-cell patch clamp recordings of MSNs from EAE corticostriatal slices show that the frequency of the glutamatergic currents was completely rescued after 1 h incubation with MAGLi. In the presence of AM281, MAGLi 432 failed to affect glutamatergic frequency (one-way ANOVA: f = 5.434, df = 58, p = 0.0023, Tukey Post-Hoc: EAE-VHL vs EAE-MAGLi p = 0.0185, EAE-MAGLi vs EAE-AM281+MAGLi p = 0.0274; CFA vs EAE-VHL p = 0.0361, CFA vs EAE-AM281+MAGLi p = 0.0479; CFA: n = 11; EAE-VHL: n = 19; EAE-MAGLi n = 16; EAE-AM281+MAGLi n = 16).

## Availability of data and materials

The datasets used and/or analysed during the current study are available from the corresponding author on reasonable request.

## Funding

The study was supported by: a F. Hoffmann -La Roche grant, Switzerland to DC by F. Hoffmann -La Roche Ltd.; Italian Ministry of Health (Ricerca Corrente IRCCS Neuromed to DC; Ricerca Corrente IRCCS San Raffaele to GM; GR-2021-12373337 to FDV and DF); Fondazione Italiana Sclerosi Multipla (FISM, Italy and co-financed with the '5 per mille' public funding, research fellowship 2020/BS/003 to FDV; CNR FOE 2020 and 2021 (Italy) project 'Nuovi Biomarker Diagnostici e Terapeutici delle Malattie Neurodegenerative' to DC and GM; #NEXT-GENERATIONEU (NGEU) and funded by the Ministry of University and Research (MUR), National Recovery and Resilience Plan (NRRP), project MNESYS (PE0000006) – A Multiscale integrated approach to the study of the nervous system in health and disease (DN. 1553 October 11, 2022) to DC, GM and AM; Private donations in memory of Veronica Tozzi to DC.

## CRediT authorship contribution statement

**Livia Guadalupi:** Writing – original draft, Supervision, Data curation, Conceptualization, Formal analysis. **Georgia Mandolesi:** Supervision, Funding acquisition, Data curation, Conceptualization. **Valentina Vanni:** Project administration, Methodology, Formal

analysis, Conceptualization. **Sara Balletta:** Methodology, Formal analysis. **Silvia Caioli:** Investigation, Formal analysis, Data curation, Methodology. **Anto Pavlovic:** Methodology, Data curation. **Francesca De Vito:** Methodology, Data curation, Formal analysis. **Diego Fresegna:** Methodology. **Krizia Sanna:** Data curation. **Laura Vitiello:** Methodology, Investigation, Formal analysis. **Monica Nencini:** Methodology, Formal analysis. **Alice Tartacca:** Methodology, Formal analysis, Data curation. **Fabrizio Mariani:** Methodology, Formal analysis, Data curation. **Valentina Rovella:** Visualization. **Sven Schippling:** Methodology, Formal analysis. **Iris Ruf:** Data curation, Methodology. **Ludovic Collin:** Data curation, Methodology. **Diego Centonze:** Conceptualization, Writing – review & editing. **Alessandra Musella:** Writing – review & editing, Writing – original draft, Supervision, Conceptualization, Data curation, Project administration.

## Declaration of competing interest

DC is the recipient of an Institutional grant from Roche. No personal compensation was received. The founding sponsors had no role in the design of the study; in the collection, analyses, or interpretation of data; in the writing of the manuscript, and in the decision to publish the results. SS, AP, IR, LC are paid employment by the company F. Hoffmann-La Roche. This does not alter the authors' adherence to all the Neuropharmacology policies on sharing data and materials. The other authors declare that they have no competing interests.

## Data availability

Data will be made available on request.

## Acknowledgments

The authors thank Massimo Tolu for helpful technical assistance, Andrea Greiter-Wilke and Theo Dinklo for contributing to the behavioral assessment of the animals and Uwe Grether for supplying the MAGL 432. The graphical abstract was created with BioRender.com.

## List of abbreviations

(2-AG) 2-Arachidonoylglycerol
(AA) arachidonic acid
(ABPP) activity-based protein profiling
AEA) anandamide
(ACSF) artificial CSF
(BBB) blood-brain barrier
(CB1) and 2 (CB2) cannabinoid receptor 1
(CNS) central nervous system
(CFA) complete Freund's Adjuvant
(dpi) day post-immunization
(ECS) endocannabinoid system
(eCBs) endocannabinoids
(EAE) experimental autoimmune encephalomyelitis
(FAAH) fatty acid amide hydrolase
(MAGLi) inhibitor of monoacylglycerol lipase
(LC/MS) liquid chromatography/mass spectrometry
(MSNs) medium spiny projection neurons
(MAGL) monoacylglycerol lipase
(MS) multiple sclerosis
(MOG35-55) myelin oligodendrocyte glycoprotein peptide 35-55
(PFA) paraformaldehyde
(PGs) prostaglandins
(sEPSC) spontaneous postsynaptic glutamatergic current
(sIPSC) spontaneous postsynaptic inhibitory current
(VHL) vehicle

## Appendix A. Supplementary data

Supplementary data to this article can be found online at https://doi.org/10.1016/j.neuropharm.2024.109940.

## References

Aharoni, R., Eilam, R., Arnon, R., 2021. Astrocytes in multiple sclerosis—essential constituents with diverse multifaceted functions. Int. J. Mol. Sci. 22 (11), 5904.
Alberti, T.B., Barbosa, W.L.R., Vieira, J.L.F., Raposo, N.R.B., Dutra, R.C., 2017. (−)-β-caryophyllene, a CB2 receptor-selective phytocannabinoid, suppresses motor paralysis and neuroinflammation in a murine model of multiple sclerosis. Int. J. Mol. Sci. 18 (4), 691.
Amici, S.A., Dong, J., Guerau-de-Arellano, M., 2017. Molecular mechanisms modulating the phenotype of macrophages and microglia. Front. Immunol. 8, 1–18.
Augusto-Oliveira, M., Arrifano, G.P., Delage, C.I., Tremblay, M.-È., Crespo-Lopez, M.E., Verkhratsky, A., 2022. Plasticity of microglia. Biol Rev Camb Philos Soc. 97 (1), 217–250.
Baecher-Allan, C., Kaskow, B.J., Weiner, H.L., 2018. Multiple sclerosis: mechanisms and immunotherapy. Neuron 97, 742–768.
Bernal-Chico, A., Canedo, M., Manterola, A., Victoria Sánchez-Gómez, M., Pérez-Samartín, A., Rodríguez-Puertas, R., Matute, C., Mato, S., 2015. Blockade of monoacylglycerol lipase inhibits oligodendrocyte excitotoxicity and prevents demyelination in vivo. Glia 63, 163–176.
Bouchet, C.A., McPherson, K.B., Coutens, B., Janowsky, A., Ingram, S.L., 2023. Monoacylglycerol lipase protects the presynaptic cannabinoid 1 receptor from desensitization by endocannabinoids after persistent inflammation. J. Neurosci. 43 (30), 5458–5467.
Brindisi, M., Maramai, S., Gemma, S., Brogi, S., Grillo, A., Di Cesare Mannelli, L., Gabellieri, E., Lamponi, S., Saponara, S., Gorelli, B., Tedesco, D., Bonfiglio, T., Landry, C., Jung, K.M., Armirotti, A., Luongo, L., Ligresti, A., Piscitelli, F., Bertucci, C., Dehouck, M.P., Campiani, G., Maione, S., Ghelardini, C., Pittaluga, A., Piomelli, D., Di Marzo, V., Butini, S., 2016. Development and pharmacological characterization of selective blockers of 2-arachidonoyl glycerol degradation with efficacy in rodent models of multiple sclerosis and pain. J. Med. Chem. 59, 2612–2632.
Carrillo-Salinas, F.J., Navarrete, C., Mecha, M., Feliú, A., Collado, J.A., Cantarero, I., Bellido, M.L., Muñoz, E., Guaza, C., 2014. A cannabigerol derivative suppresses immune responses and protects mice from experimental autoimmune encephalomyelitis. PLoS One 9 (4), e94733.
Castillo, P.E., Younts, T.J., Chávez, A.E., Hashimotodani, Y., 2012. Endocannabinoid signaling and synaptic function. Neuron 76, 70–81.
Centonze, D., Bari, M., Rossi, S., Prosperetti, C., Furlan, R., Fezza, F., De Chiara, V., Battistini, L., Bernardi, G., Bernardini, S., Martino, G., Maccarrone, M., 2007a. The endocannabinoid system is dysregulated in multiple sclerosis and in experimental autoimmune encephalomyelitis. Brain 130, 2543–2553.
Centonze, D., Muzio, L., Rossi, S., Cavasinni, F., De Chiara, V., Bergami, A., Musella, A., D'Amelio, M., Cavallucci, V., Martorana, A., Bergamaschi, A., Cencioni, M.T., Diamantini, A., Butti, E., Comi, G., Bernardi, G., Cecconi, F., Battistini, L., Furlan, R., Martino, G., 2009. Inflammation triggers synaptic alteration and degeneration in experimental autoimmune encephalomyelitis. J. Neurosci. 29, 3442–3452.
Centonze, D., Rossi, S., Prosperetti, C., Gasperi, V., De Chiara, V., Bari, M., Tscherter, A., Febbraro, F., Bernardi, G., Maccarrone, M., 2007b. Endocannabinoids limit metabotropic glutamate 5 receptor-mediated synaptic inhibition of striatal principal neurons. Mol. Cell. Neurosci. 35 (2).
Chiurchiù, V., van der Stelt, M., Centonze, D., Maccarrone, M., 2018. The endocannabinoid system and its therapeutic exploitation in multiple sclerosis: clues for other neuroinflammatory diseases. Prog Neurobiol. 160, 82–100.
Ciaramellano, F., Fanti, F., Scipioni, L., Maccarrone, M., Oddi, S., 2023. Endocannabinoid metabolism and transport as drug targets. In: Maccarrone, M. (Ed.), Endocannabinoid Signaling: Methods and Protocols. Springer US, New York, NY, pp. 201–211. https://doi.org/10.1007/978-1-0716-2728-0_16.
Compston, A., Coles, A., 2008. Multiple sclerosis. The Lancet. 372, 1502–1517.
Dendrou, C.A., Fugger, L., Friese, M.A., 2015. Immunopathology of multiple sclerosis. Nat. Rev. Immunol.15 (9) 545-558.
Deng, H., Li, W., 2020. Monoacylglycerol lipase inhibitors: modulators for lipid metabolism in cancer malignancy, neurological and metabolic disorders. Acta Pharm. Sin. B 10, 582–602..
Duffy, S.S., Hayes, J.P., Fiore, N.T., Moalem-Taylor, G., 2021. The cannabinoid system and microglia in health and disease. Neuropharmacology 190, 108555.
Ehrhart, J., Obregon, D., Mori, T., Hou, H., Sun, N., Bai, Y., Klein, T., Fernandez, F., Tan, J., Shytle, R.D., 2005. Stimulation of cannabinoid receptor 2 (CB2) suppresses microglial activation. J. Neuroinflammation 2, 29.
Eraso-Pichot, A., Pouvreau, S., Olivera-Pinto, A., Gomez-Sotres, P., Skupio, U., Marsicano, G., 2023. Endocannabinoid signaling in astrocytes. Glia 71, 44–59..
Gentile, A., De Vito, F., Fresegna, D., Rizzo, F.R., Bullitta, S., Guadalupi, L., Vanni, V., Buttari, F., Stampanoni Bassi, M., Leuti, A., Chiurchiù, V., Marfia, G.A., Mandolesi, G., Centonze, D., Musella, A., 2020. Peripheral T cells from multiple sclerosis patients trigger synaptotoxic alterations in central neurons. Neuropathol. Appl. Neurobiol. 46 (2), 160–170.
Gentile, A., Musella, A., Bullitta, S., Fresegna, D., De Vito, F., Fantozzi, R., Piras, E., Gargano, F., Borsellino, G., Battistini, L., Schubart, A., Mandolesi, G., Centonze, D., 2016. Siponimod (BAF312) prevents synaptic neurodegeneration in experimental multiple sclerosis. J. Neuroinflammation 13 (1), 207.

Grasselli, G., Rossi, S., Musella, A., Gentile, A., Loizzo, S., Muzio, L., Di Sanza, C., Errico, F., Musumeci, G., Haji, N., Fresegna, D., Sepman, H., De Chiara, V., Furlan, R., Martino, G., Usiello, A., Mandolesi, G., Centonze, D., 2013. Abnormal NMDA receptor function exacerbates experimental autoimmune encephalomyelitis. Br. J. Pharmacol. 168 (2), 502–517.

Haji, N., Mandolesi, G., Gentile, A., Sacchetti, L., Fresegna, D., Rossi, S., Musella, A., Sepman, H., Motta, C., Studer, V., De Chiara, V., Bernardi, G., Strata, P., Centonze, D., 2012. TNF-α-mediated anxiety in a mouse model of multiple sclerosis. Exp. Neurol. 237 (2), 296–303.

Hernández-Torres, G., Cipriano, M., Hedén, E., Björklund, E., Canales, Á., Zian, D., Feliú, A., Mecha, M., Guaza, C., Fowler, C.J., Ortega-Gutiérrez, S., López-Rodríguez, M.L., 2014. A reversible and selective inhibitor of monoacylglycerol lipase ameliorates multiple sclerosis. Angew. Chem. Int. Ed. 53, 13765–13770.

Kemble, A.M., Hornsperger, B., Ruf, I., Richter, H., Benz, J., Kuhn, B., Heer, D., Wittwer, M., Engelhardt, B., Grether, U., Collin, L., 2022. A potent and selective inhibitor for the modulation of MAGL activity in the neurovasculature. PLoS One 17 (9), e0268590.

Kendall, D.A., Yudowski, G.A., 2017. Cannabinoid receptors in the central nervous system: their signaling and roles in disease. Front. Cell. Neurosci. 10. Jan 4. 294.

Kinsey, S.G., Long, J.Z., O'Neal, S.T., Abdullah, R.A., Poklis, J.L., Boger, D.L., Cravatt, B. F., Lichtman, A.H., 2009. Blockade of endocannabinoid-degrading enzymes attenuates neuropathic pain. J. Pharmacol. Exp. Therapeut. 330, 902–910.

Kozela, E., Lev, N., Kaushansky, N., Eilam, R., Rimmerman, N., Levy, R., Ben-Nun, A., Juknat, A., Vogel, Z., 2011. Cannabidiol inhibits pathogenic T cells, decreases spinal microglial activation and ameliorates multiple sclerosis-like disease in C57BL/6 mice. Br. J. Pharmacol. 163, 1507–1519.

De Lago, E., Moreno-Martet, M., Cabranes, A., Ramos, J.A., Fernández-Ruiz, J., 2012. Cannabinoids ameliorate disease progression in a model of multiple sclerosis in mice, acting preferentially through CB1 receptor-mediated anti-inflammatory effects. Neuropharmacology 62, 2299–2308..

Long, J.Z., Nomura, D.K., Vann, R.E., Walentiny, D.M., Booker, L., Jin, X., Burston, J.J., Sim-Selley, L.J., Lichtman, A.H., Wiley, J.L., Cravatt, B.F., 2009. Dual blockade of FAAH and MAGL identifies behavioral processes regulated by endocannabinoid crosstalk in vivo. Proc. Natl. Acad. Sci. USA. 106 (48), 20270–20275.

Lovinger, D.M., Mathur, B.N., 2016. Chapter 10 - endocannabinoid signaling in the striatum. In: Steiner, H., Tseng, K.Y. (Eds.), Handbook of Behavioral Neuroscience, vol. 24. Elsevier, pp. 197–215.

Ma, L., Jia, J., Liu, X., Bai, F., Wang, Q., Xiong, L., 2015. Activation of murine microglial N9 cells is attenuated through cannabinoid receptor CB2 signaling. Biochem. Biophys. Res. Commun. 458, 92–97.

Mandolesi, G., Gentile, A., Musella, A., Fresegna, D., De Vito, F., Bullitta, S., Sepman, H., Marfia, G.A., Centonze, D., 2015. Synaptopathy connects inflammation and neurodegeneration in multiple sclerosis. Nat. Rev. Neurol. 11 (12), 711–724.

Mandolesi, G., Bullitta, S., Fresegna, D., De Vito, F., Rizzo, F.R., Musella, A., Guadalupi, L., Vanni, V., Stampanoni Bassi, M., Buttari, F., Viscomi, M.T., Centonze, D., Gentile, A., 2019. Voluntary running wheel attenuates motor deterioration and brain damage in cuprizone-induced demyelination. Neurobiol. Dis. 129:, 102–117.

Mangiardi, M., Crawford, D.K., Xia, X., Du, S., Simon-Freeman, R., Voskuhl, R.R., Tiwari-Woodruff, S.K., 2011. An animal model of cortical and callosal pathology in multiple sclerosis. Brain Pathol. 21, 263–278.

Montilla, A., Zabala, A., Er-Lukowiak, M., Rissiek, B., Magnus, T., Rodriguez-Iglesias, N., Sierra, A., Matute, C., Domercq, M., 2023. Microglia and meningeal macrophages depletion delays the onset of experimental autoimmune encephalomyelitis. Cell Death Dis. 14, 16.

Morrison, H., Young, K., Qureshi, M., Rowe, R.K., Lifshitz, J., 2017. Quantitative microglia analyses reveal diverse morphologic responses in the rat cortex after diffuse brain injury. Sci. Rep. 7 (1), 13211.

Musella, A., Sepman, H., Mandolesi, G., Gentile, A., Fresegna, D., Haji, N., Conrad, A., Lutz, B., Maccarrone, M., Centonze, D., 2014. Pre- and postsynaptic type-1 cannabinoid receptors control the alterations of glutamate transmission in experimental autoimmune encephalomyelitis. Neuropharmacology 79, 567–572.

Musumeci, G., Grasselli, G., Rossi, S., De Chiara, V., Musella, A., Motta, C., Studer, V., Bernardi, G., Haji, N., Sepman, H., Fresegna, D., Maccarrone, M., Mandolesi, G., Centonze, D., 2011. Transient receptor potential vanilloid 1 channels modulate the synaptic effects of TNF-α and of IL-1β in experimental autoimmune encephalomyelitis. Neurobiol. Dis. 43 (3), 669–677.

Navarrete, C., García-Martin, A., Garrido-Rodríguez, M., Mestre, L., Feliú, A., Guaza, C., Calzado, M.A., Muñoz, E., 2020. Effects of EHP-101 on inflammation and remyelination in murine models of Multiple sclerosis. Neurobiol. Dis. 143, 104994.

Nomura, D.K., Hudak, C.S.S., Ward, A.M., Burston, J.J., Issa, R.S., Fisher, K.J., Abood, M. E., Wiley, J.L., Lichtman, A.H., Casida, J.E., 2008. Monoacylglycerol lipase regulates 2-arachidonoylglycerol action and arachidonic acid levels. Bioorg. Med. Chem. Lett. 18, 5875–5878.

Nomura, D.K., Morrison, B.E., Blankman, J.L., Long, J.Z., Kinsey, S.G., Marcondes, M.C. G., Ward, A.M., Hahn, Y.K., Lichtman, A.H., Conti, B., Cravatt, B.F., 2011. Endocannabinoid hydrolysis generates brain prostaglandins that promote neuroinflammation. Science 34 (6057), 809–813.

De Petrocellis, L., Di Marzo, V., 2009. An introduction to the endocannabinoid system: from the early to the latest concepts. Best Pract. Res. Clin. Endocrinol. Metabol. 23, 1–15.

Pinto, B., Morelli, G., Rastogi, M., Savardi, A., Fumagalli, A., Petretto, A., Bartolucci, M., Varea, E., Catelani, T., Contestabile, A., Perlini, L.E., Cancedda, L., 2020. Rescuing over-activated microglia restores cognitive performance in juvenile animals of the dp (16) mouse model of down syndrome. Neuron 108, 887–904.e12.

Piomelli, D., 2003. The molecular logic of endocannabinoid signalling. Nat. Rev. Neurosci. 4, 873–884.

Piro, J.R., Suidan, G.L., Quan, J., Pi, Y., O'Neill, S.M., Ilardi, M., Pozdnyakov, N., Lanz, T. A., Xi, H., Bell, R.D., Samad, T.A., 2018. Inhibition of 2-AG hydrolysis differentially regulates blood brain barrier permeability after injury. J. Neuroinflammation 15, 142..

Pryce, G., Cabranes, A., Fernández-Ruiz, J., Bisogno, T., Di Marzo, V., Long, J.Z., Cravatt, B.F., Giovannoni, G., Baker, D., 2013. Control of experimental spasticity by targeting the degradation of endocannabinoids using selective fatty acid amide hydrolase inhibitors. Multiple Sclerosis Journal 19, 1896–1904.

Rahimi, A., Faizi, M., Talebi, F., Noorbakhsh, F., Kahrizi, F., Naderi, N., 2015. Interaction between the protective effects of cannabidiol and palmitoylethanolamide in experimental model of multiple sclerosis in C57BL/6 mice. Neuroscience 290, 279–287.

Ren, S yu, Wang, Z zhen, Zhang, Y., Chen, N hong, 2020. Potential application of endocannabinoid system agents in neuropsychiatric and neurodegenerative diseases—focusing on FAAH/MAGL inhibitors. Acta Pharmacol. Sin. 41, 1263–1271.

Ribeiro, R., Yu, F., Wen, J., Vana, A., Zhang, Y., 2013. Therapeutic potential of a novel cannabinoid agent CB52 in the mouse model of experimental autoimmune encephalomyelitis. Neuroscience 254, 427–442..

Rossi, S., Furlan, R., De Chiara, V., Motta, C., Studer, V., Mori, F., Musella, A., Bergami, A., Muzio, L., Bernardi, G., Battistini, L., Martino, G., Centonze, D., 2012. Interleukin-1β causes synaptic hyperexcitability in multiple sclerosis. Ann. Neurol. 71, 76–83.

Rossi, S., Furlan, R., Chiara, V De, Muzio, L., Musella, A., Motta, C., Studer, V., Cavasinni, F., Bernardi, G., Martino, G., Cravatt, B.F., Lutz, B., Maccarrone, M., Centonze, D., 2011. Cannabinoid CB1 receptors regulate neuronal TNF-α effects in experimental autoimmune encephalomyelitis. Brain Behav. Immun. 25, 1242–1248.

Rossi, S., Motta, C., Musella, A., Centonze, D., 2014. The interplay between inflammatory cytokines and the endocannabinoid system in the regulation of synaptic transmission. Neuropharmacology 96, 105–112.

Schlosburg, J.E., Blankman, J.L., Long, J.Z., Nomura, D.K., Pan, B., Kinsey, S.G., Nguyen, P.T., Ramesh, D., Booker, L., Burston, J.J., Thomas, E.A., Selley, D.E., Sim-Selley, L.J., Liu, Q.S., Lichtman, A.H., Cravatt, B.F., 2010. Chronic monoacylglycerol lipase blockade causes functional antagonism of the endocannabinoid system. Nat. Neurosci. 13, 1113–1119.

Stella, N., 2010. Cannabinoid and cannabinoid-like receptors in microglia, astrocytes, and astrocytomas. Glia 58, 1017–1030..

Tanaka, M., Sackett, S., Zhang, Y., 2020. Endocannabinoid modulation of microglial phenotypes in neuropathology. Front. Neurol. 11 (87).

Tao, G., Datta, S., He, R., Nelson, F., Wolinsky, J.S., Narayana, P.A., 2009. Deep gray matter atrophy in multiple sclerosis: a tensor based morphometry. J. Neurol. Sci. 282, 39–46.

Tuccinardi, T., Granchi, C., Rizzolio, F., Caligiuri, I., Battistello, V., Toffoli, G., Minutolo, F., Macchia, M., Martinelli, A., 2014. Identification and characterization of a new reversible MAGL inhibitor. Bioorg. Med. Chem. 22, 3285–3291.

Vidal-Itriago, A., Radford, R.A.W., Aramideh, J.A., Maurel, C., Scherer, N.M., Don, E.K., Lee, A., Chung, R.S., Graeber, M.B., Morsch, M., Oct 19 2022. Microglia morphophysiological diversity and its implications for the CNS. Front Immunol 13, 997786.

Yiangou, Y., Facer, P., Durrenberger, P., Chessell, I.P., Naylor, A., Bountra, C., Banati, R. R., Anand, P., 2006. COX-2, CB2 and P2X7-immunoreactivities are increased in activated microglial cells/macrophages of multiple sclerosis and amyotrophic lateral sclerosis spinal cord. BMC Neurol. 6, 12.

Young, K., Morrison, H.W., 2018. Quantifying microglia morphology from photomicrographs of immunohistochemistry prepared tissue using ImageJ. J. Vis. Exp. 136, 57648.

Zou, S., Kumar, U., 2018. Cannabinoid receptors and the endocannabinoid system: signaling and function in the central nervous system. Int. J. Mol. Sci. 19 (3), 833.